



1 **Historical (1960-2014) lightning and LNO_x trends and their** 2 **controlling factors in a chemistry–climate model**

3 Yanfeng He¹, Kengo Sudo^{1, 2}

4 ¹ Graduate School of Environment Studies, Nagoya University, Nagoya, 464-8601, Japan

5 ² Japan Agency for Marine–Earth Science and Technology (JAMSTEC), Yokohama, 237-0061, Japan

6 *Correspondence to:* Yanfeng He (hyf412694462@gmail.com)

7 **Abstract.** Lightning can cause natural disasters that engender human and animal injuries or fatalities, infrastructure
8 destruction, and wildfire ignition. Lightning-produced NO_x (LNO_x), a major NO_x (NO_x=NO+NO₂) source, plays a vital role
9 in atmospheric chemistry and global climate. The Earth has experienced marked global warming and changes in aerosol and
10 aerosol precursor emissions (AeroPEs) since the 1960s. Investigating long-term historical (1960–2014) lightning and LNO_x
11 trends can provide important indicators for all lightning-related phenomena and for LNO_x effects on atmospheric chemistry
12 and global climate. Understanding how global warming and changes in AeroPEs influence historical lightning–LNO_x trends
13 is also helpful because it can provide a scientific basis for assessing future lightning–LNO_x trends. Moreover, global
14 lightning activities' responses to large volcanic eruptions (such as the 1991 Pinatubo eruption) are not well elucidated, and
15 are worth exploring. This study used the widely used cloud top height lightning scheme (CTH scheme) and the newly
16 developed ice-based ECMWF-McCAUL lightning scheme to investigate historical (1960–2014) lightning–LNO_x trends and
17 variations and their controlling factors (global warming, increases in AeroPEs, and Pinatubo eruption) in the framework of
18 the CHASER (MIROC) chemistry–climate model. Results of sensitive experiments indicate that both lightning schemes
19 simulated almost flat global mean lightning flash rate trends during 1960–2014 in CHASER. Moreover, both lightning
20 schemes suggest that past global warming enhances historical trends of global mean lightning density and global LNO_x
21 emissions in a positive direction (around 0.03% yr⁻¹ or 3% K⁻¹). However, past increases in AeroPEs exert an opposite effect
22 to the lightning–LNO_x trends (-0.07% yr⁻¹ – -0.04% yr⁻¹ for lightning and -0.08% yr⁻¹ – -0.03% yr⁻¹ for LNO_x). Additionally,
23 effects of past global warming and increases in AeroPEs on lightning trends were found to be heterogeneous across different
24 regions when analyzing lightning trends on the global map. Lastly, this study is the first to suggest that global lightning
25 activities were suppressed markedly during the first year after the Pinatubo eruption shown in both lightning schemes (global
26 lightning activities decreased by as much as 17.02% simulated by the ECMWF-McCAUL scheme). Based on the simulated
27 suppressed lightning activities after the Pinatubo eruption, our study also indicates that global LNO_x emissions decreased
28 after the Pinatubo eruption (2.41%–8.72% for the annual percentage reduction), which lasted 2–3 years. Model
29 intercomparisons of lightning flash rate trends and variations between our study (CHASER) and other Coupled Model
30 Intercomparison Project Phase 6 (CMIP6) models indicate significant uncertainties in historical (1960–2014) global
31 lightning trend simulations. Such uncertainties must be investigated further.



32 **1 Introduction**

33 Lightning, an extremely energetic natural phenomenon, always occurs somewhere on Earth: its average occurrence
34 frequency is approximately 46 times per second (Cecil et al., 2014). Lightning generation is associated with electric charge
35 separation, which is mainly realized by collisions between graupel and hail and other types of hydrometeors within
36 convective clouds (Lopez, 2016). As a natural disaster, lightning can cause human and animal injuries or fatalities,
37 infrastructure destruction, and wildfire ignition (Cervený et al., 2017; Cooper and Holle, 2019; Jensen et al., 2022;
38 Veraverbeke et al., 2022). Lightning-produced NO_x (LNO_x) accounts for around 10% of the global tropospheric NO_x
39 ($\text{NO}_x = \text{NO} + \text{NO}_2$) source. It is regarded as the dominant NO_x source in the middle to upper troposphere (Schumann and
40 Huntrieser, 2007; Finney et al., 2016b). LNO_x plays a vital role in atmospheric chemistry and global climate by controlling
41 the abundances of OH radical, important greenhouse gases (GHGs) such as ozone and methane, and other trace gases
42 (Labrador et al., 2005; Schumann and Huntrieser, 2007; Wild, 2007; Liaskos et al., 2015; Finney et al., 2016a; Murray,
43 2016; Tost, 2017; He et al., 2022b).

44

45 Reportedly, the lightning flash rate is related to the stage of convective cloud development (Williams et al., 1989),
46 Convective Available Potential Energy (CAPE) (Romps et al., 2014), cloud liquid–ice water content (Saunders et al., 1991;
47 Finney et al., 2014), and even the convective precipitation volume (Goodman et al., 1990; McCaul et al., 2009; Romps et al.,
48 2014). Long-term global warming is associated with changes in the overall temperature and relative humidity profiles in the
49 atmosphere and global convective adjustment (Manabe and Wetherald, 1975; Del Genio et al., 2007), which can strongly
50 affect the lightning-related factors described above. Consequently, long-term global warming can be a crucially important
51 factor affecting long-term variations in global lightning activity. Many earlier numerical studies manifest that global
52 lightning activities are sensitive to long-term global warming, with most studies showing 5–16% (average around 10%)
53 increases in global lightning activities per 1 K global warming (Price and Rind, 1994; Zeng et al., 2008; Hui and Hong,
54 2013; Banerjee et al., 2014; Krause et al., 2014; Clark et al., 2017). However, minor numerical studies such as using an ice-
55 based lightning scheme or convective mass flux as a proxy to parameterize lightning have yielded opposite results (global
56 lightning activity will decrease under long-term global warming) (Clark et al., 2017; Finney et al., 2018).

57

58 Aside from long-term global warming, changes in aerosol loading can also be responsible for long-term global lightning
59 activity variations. Aerosols influence lightning activity through aerosol radiative and microphysical effects, but the degree
60 to which the two distinct effects influence regional or global scale lightning activities remains unclear (Yuan et al., 2011;
61 Yang et al., 2013; Tan et al., 2016; Altaratz et al., 2017; Wang et al., 2018; Liu et al., 2020). Further research is needed. It is
62 urgently necessary to elucidate the effects of aerosol radiative and microphysical effects on lightning on a global scale. The
63 aerosol radiative effects indicate that aerosols can heat the atmospheric layer and can cool the Earth's surface by absorbing
64 and scattering solar radiation (Kaufman et al., 2002; Koren et al., 2004, 2008; Li et al., 2017). Thereby, convection and



65 electrical activities are likely to be inhibited (Koren et al., 2004; Yang et al., 2013; Tan et al., 2016). The microphysical
66 effects suggest that by acting as cloud condensation nuclei (CCN) or as ice nuclei, aerosols can reduce the mean size of
67 cloud droplets, thereby suppressing the coalescence of cloud droplets into raindrops. Consequently, more liquid water
68 particles are uplifted to higher mixed-phase regions of the troposphere, where they invigorate lightning (Wang et al., 2018;
69 Liu et al., 2020).

70

71 The Earth has experienced significant global warming and changes in AeroPEs since the 1960s (Hoesly et al., 2018; Climate
72 at a Glance | National Centers for Environmental Information (NCEI), 2022). However, how historical lightning has trended
73 and how lightning has responded to historical global warming and changes in AeroPEs are not well examined. This topic is
74 worth exploring because historical lightning densities are indicators for all lightning-related phenomena (Price and Rind,
75 1994). Exploring the historical global LNO_x emission trend is also meaningful because it can indicate the effects of LNO_x
76 emissions on atmospheric chemistry and global climate. Furthermore, investigating the effects of historical global warming
77 and increases in AeroPEs on historical lightning–LNO_x trends can provide a basis for assessing future lightning–LNO_x
78 trends.

79

80 Large-scale volcanic eruptions such as the 1991 Pinatubo eruption inject tremendous amounts of sulfuric gas into the
81 stratosphere, where it converts to H₂SO₄ aerosols. Consequently, the size of the stratospheric aerosol layer is increased. The
82 enhanced stratospheric aerosol layer can cool the Earth's surface heterogeneously and can decrease the total amount of water
83 in the atmosphere (Soden et al., 2002; Boucher, 2015, p.63). The near-global perturbations in the radiative energy balance
84 and meteorological fields caused by such strong volcanic eruptions might influence global lightning activities. If so, there
85 might be ramifications for all lightning-related phenomena. Nevertheless, they remain poorly understood.

86

87 In our earlier work, we developed a new process and ice-based lightning scheme called the ECMWF-McCAUL scheme (He
88 et al., 2022b). This lightning scheme was developed by combining benefits of the lightning scheme used in the European
89 Centre for Medium-Range Weather Forecasts (ECMWF) forecasting system (Lopez, 2016) and those presented by
90 McCaul's work (McCaul et al., 2009). The ECMWF-McCAUL scheme simulated the best lightning density spatial
91 distributions among four existing lightning schemes when compared against satellite lightning observations (Lightning
92 Imaging Sensor (LIS) and Optical Transient Detector (OTD)). The sensitivity of global lightning activity to changes in
93 surface temperature on a decadal timescale is estimated as 10.13% K⁻¹ by the ECMWF-McCAUL scheme (He et al., 2022b),
94 which is close to most past estimates (average around 10% K⁻¹).

95

96 Using a chemistry–climate model CHASER (MIROC) with two lightning schemes (the widely used cloud top height scheme
97 and the ice-based ECMWF-McCAUL scheme), we quantitatively investigated historical lightning–LNO_x trends and found
98 how global warming, increases in AeroPEs, and how the Pinatubo eruption respectively influenced them. Using two



99 lightning schemes, we demonstrated the sensitivities of different lightning schemes to historical global warming, increases in
100 AeroPEs, and the Pinatubo eruption.

101

102 Research methods, including the model description and experiment setup, are described in Sect. 2. In Sect. 3.1, the simulated
103 historical lightning distributions and trends are validated with LIS/OTD lightning observations. Section 3.2 presents the
104 effects of global warming and increases in AeroPEs on historical lightning–LNO_x trends. In Sect. 3.3, the effects of the
105 Pinatubo volcanic eruption on historical lightning–LNO_x trends are discussed. Section 3.4 elucidated model
106 intercomparisons of lightning flash rate trends and variation between our study (CHASER) and other CMIP6 model outputs.
107 Section 4 presents relevant discussions and conclusions obtained from this study.

108 2 Method

109 2.1 Chemistry–climate model

110 We used the CHASER (MIROC) global chemistry–climate model (Sudo et al., 2002; Sudo and Akimoto, 2007; Watanabe et
111 al., 2011; Ha et al., 2021) for this study, which incorporated consideration of detailed chemical and physical processes in the
112 troposphere and stratosphere. The CHASER version adopted for this study simulates the distributions of 94 chemical species
113 while reflecting the effects of 269 chemical reactions (58 photolytic, 190 kinetic, and 21 heterogeneous). As processes
114 associated with tropospheric chemistry, Non-Methane Hydrocarbons (NMHC) oxidation and the fundamental chemical cycle
115 of O_x–NO_x–HO_x–CH₄–CO are considered. CHASER simulates stratospheric chemistry involving the Chapman mechanisms
116 and catalytic reactions associated with HO_x, NO_x, ClO_x, and BrO_x. Moreover, it simulates the formation of polar
117 stratospheric clouds (PSCs) and the heterogeneous reactions occurring on their surfaces. CHASER is on-line-coupled to
118 MIROC AGCM ver. 5.0 (Watanabe et al., 2011), which simulates cumulus convection (Arakawa–Schubert scheme) and
119 grid-scale large-scale condensation to represent cloud and precipitation processes. The radiation flux is calculated using a
120 two-stream k distribution radiation scheme, which considers absorption, scattering, and emissions by aerosol and cloud
121 particles as well as by gaseous species (Goto et al., 2015). The aerosol component in CHASER is coupled with the
122 SPRINTARS aerosol model (Takemura et al., 2009), particularly for simulating primary organic carbon, sea-salt, and dust,
123 which is also based on MIROC. The aerosol radiation effects are considered in both large-scale condensation and cumulus
124 convection schemes, although the aerosol microphysical effects are only reflected in the large-scale condensation scheme.

125

126 This study used a horizontal resolution of T42 (2.8° × 2.8°), with vertical resolution of 36 σ-p hybrid levels from the surface
127 to approximately 50 km. Anthropogenic and biomass burning emissions were obtained from the CMIP6 forcing datasets
128 (van Marle et al., 2017; Hoesly et al., 2018) for 1959–2014 (<https://esgf-node.llnl.gov/search/input4mips/>, last access: 19
129 September 2022). Interannual variation in biogenic emissions for isoprene, monoterpene, acetone, and methanol, were
130 considered using an off-line simulation by the Vegetation Integrative Simulator for Trace Gases (VISIT) terrestrial



131 ecosystem model (Ito and Inatomi, 2012). The residual biogenic emissions (ethane, propane, ethylene, propene) used are
132 climatological values derived from the Model of Emissions of Gases and Aerosols from Nature (MEGAN) modeling system
133 (Guenther et al., 2012).

134

135 The CHASER (MIROC) global chemistry–climate model originally parameterizes lightning with the widely used cloud top
136 height scheme (Price and Rind, 1992). A newly developed ice-based lightning scheme called the ECMWF-McCAUL here
137 had been implemented into CHASER (MIROC) (He et al., 2022b). The ECMWF-McCAUL scheme computes lightning
138 flash rates as a function of CAPE and column precipitating ice (including cloud ice, graupel, and snow). Compared with the
139 cloud top height, a salient advantage of the ECMWF-McCAUL scheme is that it has a direct physical link with the charging
140 mechanism.

141 2.2 Lightning NO_x emission parameterizations

142 We tested two lightning schemes for this study. The first lightning scheme is the widely used cloud top height (CTH) scheme
143 (Price and Rind, 1992), which was originally used in CHASER (MIROC). This lightning scheme calculates the lightning
144 flash rate using the following equations.

$$145 F_l = 3.44 \times 10^{-5} H^{4.9} \quad (1)$$

$$146 F_o = 6.2 \times 10^{-4} H^{1.73} \quad (2)$$

147 Therein, F represents the total flash frequency (fl. min⁻¹), H stands for the cloud-top height (km), and subscripts l and o
148 respectively denote the land and ocean (Price and Rind, 1992). Actually, we realize the CTH scheme in CHASER using the
149 following equations (Eq. (3) and Eq. (4)). Each model layer's cumulus cloud fractions are used to weight the calculated
150 lightning densities from that layer in the CTH scheme.

$$151 F_l = \sum_{i=1}^{n=36} adj_factor \times Cu_CF_i \times (H_i - H_{surface})^{4.9} \quad (3)$$

$$152 F_o = \sum_{i=1}^{n=36} adj_factor \times Cu_CF_i \times (H_i - H_{surface})^{1.73} \quad (4)$$

153 In those equations, i denotes the model layer index. Also, adj_factor represents adjustment factors that differ for different
154 model layers and model grids. Cu_CF_i symbolizes cumulus cloud fraction at model layer i . H_i and $H_{surface}$ respectively
155 denote the altitude of model layer i and the altitude of the model's surface layer.

156

157 The second lightning scheme used for this study is a newly developed one named the ECMWF-McCAUL scheme (He et al.,
158 2022b), which is based on the original ECMWF scheme and findings reported by McCaul et al. (2009). The ECMWF-
159 McCAUL scheme calculates lightning flash rates as a function of CAPE (m² s⁻²) and column precipitating ice (Q_{Ra}) as

$$160 f_l = \alpha_l Q_{Ra} CAPE^{1.3} \quad (5)$$

$$161 f_o = \alpha_o Q_{Ra} CAPE^{1.3} \quad (6)$$



162 where f_l and f_o respectively symbolize the total flash density ($\text{fl. m}^{-2} \text{ s}^{-1}$) over land and ocean. In addition, α_l and α_o are
163 constants ($\text{fl. s}^{1.6} \text{ kg}^{-1} \text{ m}^{-2.6}$) determined after calibration against LIS/OTD climatology, respectively, for land and ocean.
164 For this study, α_l and α_o are set respectively to 2.67×10^{-16} and 1.68×10^{-17} . In the charge separation region (from 0° to
165 -25°C isotherm), Q_{Ra} (kg m^{-2}) is expressed as a proxy for the charging rate because of collisions between graupel and
166 hydrometeors of other types (McCaul et al., 2009). Moreover, Q_{Ra} represents the total volumetric amount of precipitating ice
167 within the charge separation region, calculated as

$$168 \quad Q_{Ra} = \int_{z_0}^{z-25} (q_{graup} + q_{snow} + q_{ice}) \bar{\rho} dz, \quad (7)$$

169 where q_{graup} , q_{snow} , and q_{ice} respectively represent the mass mixing ratios (kg kg^{-1}) of graupel, snow, and cloud ice. Also,
170 q_{ice} was diagnosed using Arakawa–Schubert cumulus parameterization. Then, q_{graup} and q_{snow} were computed at each
171 vertical level of the model using the following equations.

$$172 \quad q_{graup} = \beta \frac{P_f}{\bar{\rho} V_{graup}} \quad (8)$$

$$173 \quad q_{snow} = (1 - \beta) \frac{P_f}{\bar{\rho} V_{snow}} \quad (9)$$

174 In those equations, P_f represents the vertical profile of the frozen precipitation convective flux ($\text{kg m}^{-2} \text{ s}^{-1}$), $\bar{\rho}$ denotes the
175 air density (kg m^{-3}), and V_{graup} and V_{snow} respectively express the typical fall speeds for graupel and snow set to 3.1 and 0.5
176 m s^{-1} for this study. For land, the dimensionless coefficient β is set as 0.7, while for oceans, it is set to 0.45, to consider the
177 observed lower graupel content over the oceans.

178

179 Based on the cold cloud depth, a fourth-order polynomial (equation 10) is used to calculate the proportion of total flashes
180 that are cloud-to-ground (p). An earlier report of the literature describes the method (Price and Rind, 1993).

$$181 \quad p = \frac{1}{64.9 - 36.54D + 7.493D^2 - 0.648D^3 + 0.021D^4} \quad (10)$$

182 The depth of the cloud above the 0°C isotherms is represented by D (km) in that equation.

183

184 According to recent studies, the intra-cloud (IC) lightning flashes are as efficient as cloud-to-ground (CG) lightning flashes
185 at producing NO_x . The lightning NO_x production efficiency is estimated as 100–400 mol per flash (Ridley et al., 2005;
186 Cooray et al., 2009; Ott et al., 2010; Allen et al., 2019). The LNO_x production efficiency for IC and CG are therefore set to
187 the same value (250 mol per flash) in CHASER, which is the median of the commonly cited range of 100–400 mol per flash.
188 Consequently, the distinctions between IC and CG do not affect the distribution or magnitude of LNO_x emissions in this
189 study. It is noteworthy that marked uncertainties are involved in determining the LNO_x production efficiency (Allen et al.,
190 2019; Bucsela et al., 2019). The choice of different LNO_x production efficiency might affect the simulation of LNO_x
191 emissions. Further research must be undertaken to implement and validate a more sophisticated parameterization of LNO_x
192 production efficiency in chemistry–climate models. The calculated total column LNO_x for each grid was distributed into
193 each model layer based on a prescribed “backward C-shaped” LNO_x vertical profile (Ott et al., 2010).



194 **2.3 Lightning observation data for model evaluation**

195 We used LIS/OTD gridded climatology datasets for this study, consisting of climatologies of total lightning flash rates
196 observed using the Lightning Imaging Sensor (LIS) and Optical Transient Detector (OTD). The OTD aboard the MicroLab-1
197 satellite and LIS aboard the Tropical Rainfall Measuring Mission (TRMM) satellite (Cecil et al., 2014). Both sensors detect
198 lightning by monitoring pulses of illumination produced by lightning in the 777.4 nm atomic oxygen multiplet above
199 background levels. In low Earth orbit, both sensors view Earth locations for approximately 3 min during the pass of the OTD
200 or 1.5 min during passing of the LIS. OTD and LIS orbit the globe 14 times and 16 times a day, respectively. OTD observed
201 data between +75 and -75° latitude during May 1995 through March 2000, whereas LIS collected data between +38 and -38°
202 latitude during January 1998 through April 2015. This study uses the LIS/OTD 2.5 Degree Low Resolution Time Series
203 (LRTS). LRTS provides daily lightning flash rates on a 2.5° regular latitude–longitude grid for May 1995 through April
204 2015.

205 **2.4 CMIP6 model outputs for model comparison**

206 For the comparison of different model outputs from our study (CHASER) and other Earth system models or chemistry–
207 climate models, we used the lightning flash rate and surface temperature data from the CMIP6 CMIP Historical experiments
208 from CESM2-WACCM (Danabasoglu, 2019), GISS-E2-1-G (Kelley et al., 2020), and UKESM1-0-LL (Tang et al., 2019).
209 CESM2-WACCM uses the Community Earth System Model ver. 2 (Danabasoglu et al., 2020). The CESM2 is an open-
210 source fully coupled Earth system model. The Whole Atmosphere Community Climate Model ver. 6 (WACCM6) is the
211 atmospheric component coupled to the other components in CESM2. The GISS-E2-1-G is the NASA Goddard Institute for
212 Space Studies (GISS) chemistry–climate model version E2.1 based on the GISS Ocean v1 (G01) model (Miller et al., 2014;
213 Kelley et al., 2020). The UKESM1-0-LL is the UK's Earth system model, details of which are described by Sellar et al.
214 (2019). We used 3 ensembles from CESM2-WACCM, 9 ensembles from GISS-E2-1-G, and 18 ensembles from UKESM1-
215 0-LL. Table S1 presents all the ensemble members used for this study.

216 **2.5 Experiment setup**

217 We have conducted six sets of experiments with each set of experiments conducted using both the ECMWF-McCAUL
218 (abbreviated as F1) and CTH (abbreviated as F2) schemes. Table 1 presents the major settings of all experiments with the
219 relative explanations of those settings. STD-F1/F2 are standard experiments with the simulation period of 1959–2014. They
220 are aimed at reproducing the historical trends of lightning and LNO_x. Climate1959-F1/F2 are experiments that keep the
221 climate simulations fixed to 1959 to derive the effects of global warming on historical lightning trends. ClimateAero1959-
222 F1/F2 are intended to reflect the conditions with climate and aerosol and aerosol precursors (BC, OC, NO_x, SO₂) emissions
223 fixed to 1959. The Aero1959-F1/F2 experiments are the same as the STD-F1/F2 experiments, except for the AeroPEs fixed
224 to 1959. The fifth set of experiments (Volca-off-F1/F2) was intended to exclude the influences of the Pinatubo volcanic



225 eruption to compare to the STD-F1/F2 and to evaluate the effects of the Pinatubo eruption on historical lightning–LNO_x
226 trends and variation.

227

228 We simulate volcanic aerosol forcing by considering the prescribed stratospheric aerosol extinction in the radiation scheme.
229 We used the NASA Goddard Institute for Space Studies (GISS) (Sato et al., 1993) and Chemistry–climate Model Initiative
230 (CCMI) (Arfeuille et al., 2013) stratospheric aerosol dataset as the stratospheric aerosol climate data. To remove the volcanic
231 perturbation but maintain the stratospheric background aerosol in the Volca-off-F1/F2, we used the three-sigma rule to
232 process the Stratospheric Aerosol Climatology (SAC) during June 1991 – May 1994 using the following equation. The three-
233 sigma rule is often used to detect the outliers. This rule is appropriate to use here to discern the outliers (the perturbation of
234 SAC caused by a strong volcanic eruption).

$$235 \mathbf{SAC}_{no_pinatubo} = \begin{cases} \mathbf{SAC}_{background}, & |\mathbf{SAC}_{raw} - \mathbf{SAC}_{background}| > 3\sigma, \\ \mathbf{SAC}_{raw}, & |\mathbf{SAC}_{raw} - \mathbf{SAC}_{background}| \leq 3\sigma \end{cases} \quad (11)$$

236 In that equation, $\mathbf{SAC}_{no_pinatubo}$ denotes the stratospheric aerosol climatological data as input data for Volca-off-F1/F2
237 experiments, $\mathbf{SAC}_{background}$ represents the stratospheric background aerosol climatological data (For this study,
238 $\mathbf{SAC}_{background}$ is the corresponding averaged values of the NSAS GISS and CCMI stratospheric aerosol dataset
239 during 2001–2010, when the stratosphere was less affected by volcanic eruptions). \mathbf{SAC}_{raw} stands for the original
240 values of NSAS GISS and CCMI stratospheric aerosol dataset during June 1991 – May 1994. Moreover, σ symbolizes
241 the standard deviations of stratospheric background aerosol climate data (For this study, σ are the corresponding
242 standard deviations of NSAS GISS and CCMI stratospheric aerosol dataset during 2001–2010). Furthermore, the
243 influences of the Pinatubo eruption also affected the HadISST SSTs/sea ice fields. To remove Pinatubo eruption's
244 influences in the SSTs/sea ice fields in the Volca-off experiments also, we replace the 1991-06 – 1995-05 SSTs/sea ice
245 data with HadISST SSTs/sea ice climatological data during 1985–1990 when conducting the Volca-off experiments.
246 The 1985–1990 period was chosen because it is close to the period of 1991-06 – 1995-05 and because the SSTs/sea ice
247 fields were less affected by volcanic activity during 1985–1990.

248

249 All the experiments calculate the LNO_x emissions rates interactively by LNO_x emission parameterizations except STD-
250 rVolcaoff experiments. The STD-rVolcaoff experiments are the same as the STD experiments except for reading the
251 daily LNO_x emission rates calculated from the Volca-off experiments. The STD-rVolcaoff experiments are conducted
252 for comparison with STD experiments to elucidate the effects of the changed LNO_x emissions caused by the Pinatubo
253 eruption on atmospheric chemistry (typically methane lifetime).

254

255

256



257

Table 1: All experiments conducted for this study

Name of experiment	Period	Climate (SSTs, sea ice, GHGs) ^a	Anthropogenic and biomass burning emissions	Biogenic emissions	Stratospheric aerosol climatology
STD-F1/F2 ^b	1959–2014	1959–2014	CMIP6 1959–2014		NSAS GISS and CCM1 stratospheric aerosol dataset ^c
Climate1959-F1/F2	1959–2014	Fixed to 1959 ^d	CMIP6 1959–2014	VISIT and	As above
ClimateAero1959-F1/F2	1959–2014	Fixed to 1959	AeroPEs fixed to 1959 ^e	MEGAN ^f	As above
Aero1959-F1/F2	1959–2014	1959–2014	AeroPEs fixed to 1959		As above
Volca-off-F1/F2	1990–1999	1990–1999 ^g	CMIP6 1990–1999		Same dataset with volcanic perturbation removed
STD-rVolcaoff-F1/F2	1990–1999	All settings are the same as those used for STD experiment except for reading of the daily LNO _x emission rates calculated from the Volca-off experiments			

258 ^a For the model simulations, the climate is simulated by the prescribed SSTs/sea ice fields and the prescribed varying
 259 concentrations of GHGs (CO₂, N₂O, methane, chlorofluorocarbons – CFCs – and hydrochlorofluorocarbons – HCFCs) used
 260 only in the radiation scheme. The SSTs/sea ice fields are obtained from the HadISST dataset (Rayner et al., 2003). The
 261 prescribed GHGs concentrations are derived from CMIP6 forcing datasets (Meinshausen et al., 2017)

262 ^b We use “F1” to stand for the ECMWF-McCAUL scheme; “F2” represents the CTH scheme.

263 ^c Stratospheric aerosol radiative forcing is simulated using the prescribed stratospheric aerosol extinction, which is obtained
 264 from the NASA GISS (Sato et al., 1993) and CCM1 (Arfeuille et al., 2013) stratospheric aerosol dataset.

265 ^d The climate is fixed to 1959 for the whole simulation period using the 1959 SSTs/sea ice field and GHG concentrations
 266 during the simulation period.

267 ^e Aerosol (BC, OC) and aerosol precursors (NO_x, SO₂) emissions (anthropogenic + biomass burning) are fixed to 1959
 268 throughout the simulation period.

269 ^f Several biogenic emissions are interannually varying, including isoprene, monoterpenes, acetone, and methanol, which
 270 were calculated using an off-line simulation by the Vegetation Integrative Simulator for Trace Gases (VISIT) terrestrial
 271 ecosystem model (Ito and Inatomi, 2012). Some other reactive biogenic VOCs (ethane, propane, ethylene, propene) used are
 272 climatological data derived from the Model of Emissions of Gases and Aerosols from Nature (MEGAN) modeling system
 273 (Guenther et al., 2012).

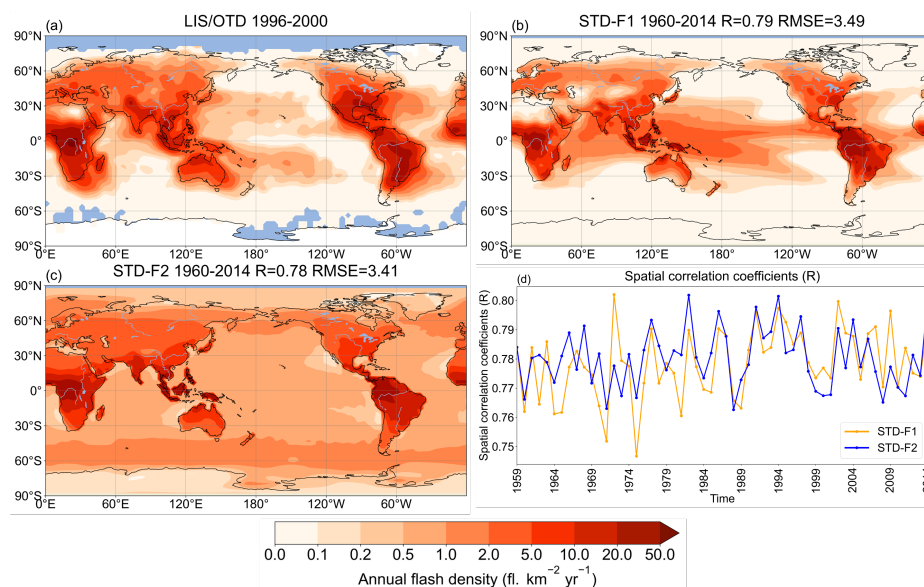


274 [§] Here the 1991-06 – 1995-05 SSTs/sea ice data were replaced with HadISST SSTs/sea ice climatological data during
 275 1985–1990.

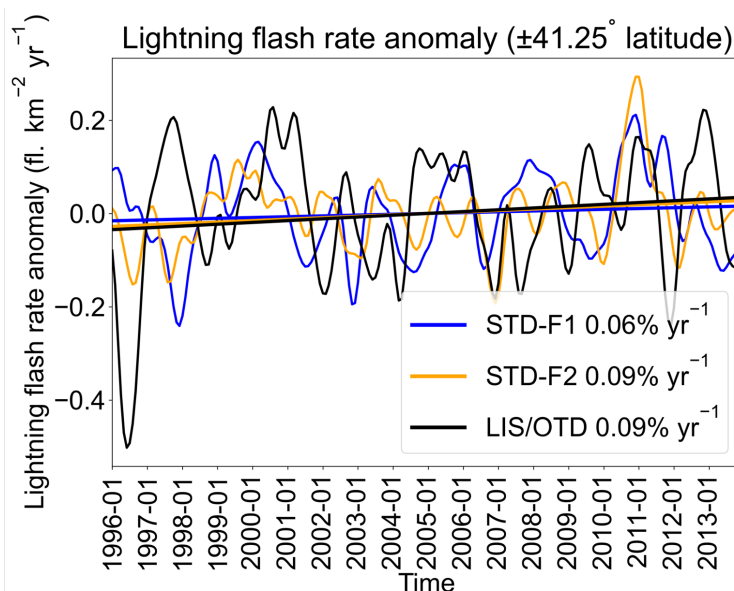
276 3 Results and Discussion

277 3.1 Validation of the simulated historical lightning distribution and trend

278 To increase the credibility of the conclusions obtained based only on the numerical simulations, the model calculations must
 279 be evaluated using observational data. We used the LIS/OTD observations to evaluate the spatial distribution and historical
 280 lightning trends simulated by CHASER (MIROC). Figures 1a–c show the annual mean spatial distribution of lightning
 281 observed by LIS/OTD and from model simulations using the ECMWF-McCAUL and CTH schemes. Both the ECMWF-
 282 McCAUL and CTH schemes generally captured the hotspots of lightning (Central Africa, Maritime Continent, South
 283 America), with strong spatial correlations between observations and model simulations ($R > 0.75$). Figure 1d exhibits strong
 284 spatial correlation between observations and simulation results maintained throughout the simulation period (1959–2014).



285
 286 **Figure 1: Annual mean lightning flash densities from (a) LIS/OTD satellite observations spanning 1996–2000, (b) the STD**
 287 **experiment (1960–2014) with the ECMWF-McCAUL scheme used, (c) the STD experiment (1960–2014) with the CTH scheme**
 288 **used. R and RMSE shown in the titles of (b) and (c) are calculated between (b)-(c) and (a). (d) presents the spatial correlation**
 289 **coefficients between modeled annual mean lightning densities of each year and LIS/OTD lightning climatologies during 1996–2000.**



290

291 **Figure 2: Lightning flash rate anomalies of 1996–2013 within $\pm 41.25^\circ$ latitude obtained from two numerical experiments (STD-F1**
 292 **and STD-F2) and LIS/OTD satellite observations. Curves represent the monthly time-series data of the $\pm 41.25^\circ$ latitude mean**
 293 **lightning flash rate anomalies with the 1-D Gaussian (Denosing) Filter applied. Lines are the fitting curves of the monthly time-**
 294 **series data of the $\pm 41.25^\circ$ latitude mean lightning flash rate anomalies. Trends of the lightning flash rate anomalies in $\% \text{ yr}^{-1}$ are**
 295 **also shown in the legends.**

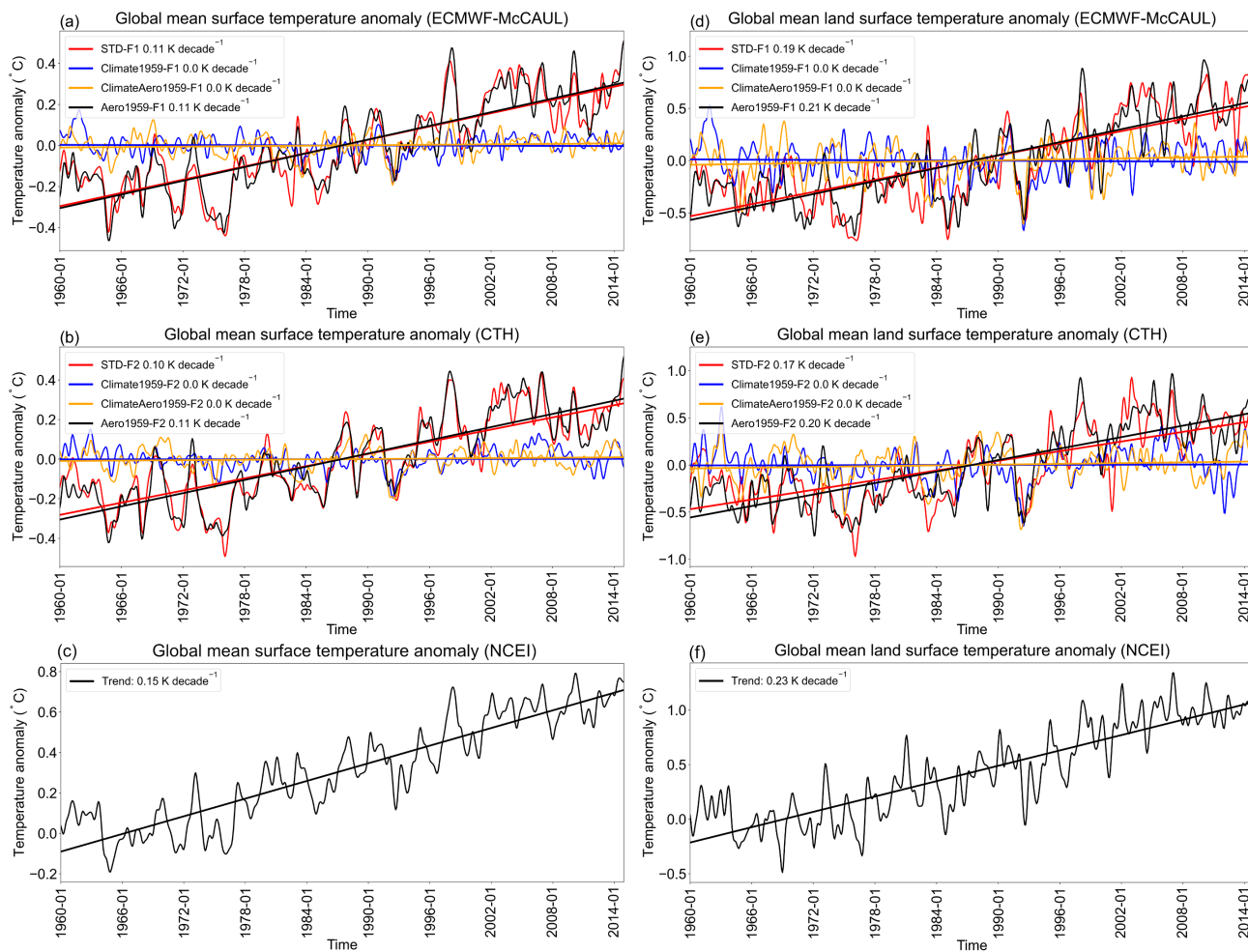
296

297 The LIS/OTD observations are also used to evaluate historical lightning trends simulated by CHASER (MIROC). Because
 298 almost all valid LIS/OTD observations exist only within $\pm 41.25^\circ$ latitude during 1996–2013, we examined the $\pm 41.25^\circ$
 299 latitude mean lightning flash rate anomaly (1996–2013) calculated from LIS/OTD observations and STD-F1/F2 numerical
 300 experiments (Fig. 2). We also note some missing values within the $\pm 41.25^\circ$ latitude in LIS/OTD observations. To keep the
 301 comparisons between observations and simulations like-for-like, when we encounter a missing value in the LIS/OTD
 302 observations during spatial averaging, we also treat the CHASER simulated value at the same location as a missing value. As
 303 displayed in Fig. 2, even when the interannual variations of the lightning flash rate anomaly sometimes differ between
 304 observations and simulations, the overall trends of lightning flash rate anomaly simulated by both schemes well matched the
 305 LIS/OTD observations. Neither the lightning flash rate anomaly (within $\pm 41.25^\circ$ latitude) derived from LIS/OTD
 306 observations nor simulations show a significant trend for 1996–2013 using the Mann–Kendall rank statistic test (significance
 307 set as 5%). The global lightning flash rate anomaly (1993–2013) obtained from simulations (STD-F1/F2) also show no
 308 significant trend, which is consistent with the Schuman Resonance (SR) intensity observations (1993–2013) at Rhode Island,
 309 USA (Earle Williams, 2022). However, the SR observations in Rhode Island (USA) exclude consideration of the influences
 310 of solar cycles, which makes it less appropriate for lightning trend evaluation.



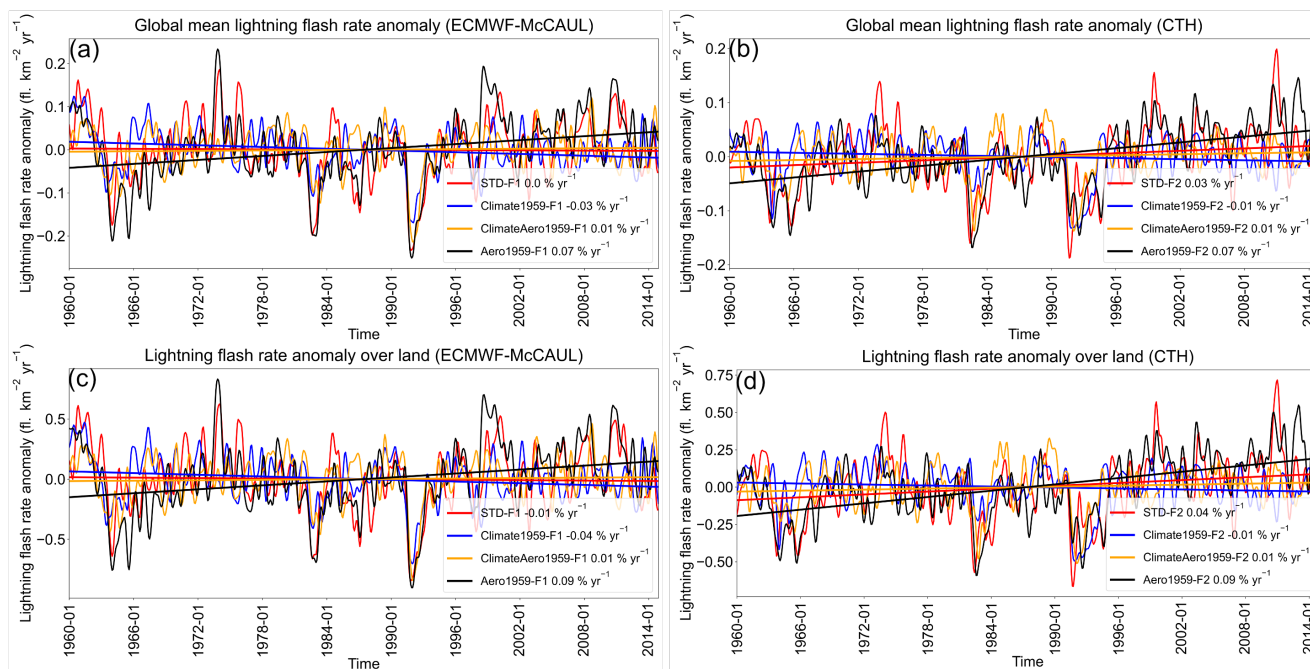
311 **3.2 Effects of global warming and increases in AeroPEs on historical lightning–LNO_x trends**

312 As introduced in Sect. 1, global warming and changes in AeroPEs are the two main factors which influence the long-term
313 (1960-2014) historical lightning trends (Hereinafter, historical lightning trends indicate lightning trends of 1960–2014.). To
314 analyze the effects of global warming on historical lightning trends, we designed and conducted two sets of experiments: one
315 set of experiments including “global warming” (STD-F1/F2) and another set of experiments excluding “global warming”
316 (Climate1959-F1/F2). Figures 3a and 3b respectively depict the global surface temperature anomalies calculated from the
317 ECMWF-McCAUL and CTH schemes. The STD and Aero1959 experiments show an increasing trend (around 0.11 K
318 decade⁻¹) of global mean surface temperature anomalies, which is close to the trend (around 0.15 K decade⁻¹) obtained from
319 NOAA’s National Centers for Environmental Information (NCEI). Global temperature change data from 1880 to the present
320 are available from the NCEI, which tracks the variations of the Earth’s temperature based on thousands of stations’
321 observation data around the globe (Climate at a Glance | National Centers for Environmental Information (NCEI), 2022).
322 When the prescribed SSTs/sea ice fields and GHGs concentrations were fixed to 1959 throughout the simulation period, the
323 simulated trends of global mean surface temperature anomalies turned out to be flat (Climate1959 and ClimateAero1959).
324 To elucidate the effects of increases in AeroPEs on averaged surface temperature to the greatest extent possible, we also
325 show the averaged surface temperature anomaly only over land regions (Figs. 3d–f). The simulated global mean land surface
326 temperature anomalies are also well-matched with the NCEI observational data. The aerosol cooling effect can be more
327 evident when only particularly addressing surface temperature trends averaged over land (Figs. 3d–e).



328

329 **Figure 3: Monthly time-series data of global mean surface temperature anomalies with 1-D Gaussian (Denosing) Filter applied**
 330 **and their fitting curves calculated from the outputs of numerical experiments (a–b) and obtained from NCEI (c). Figures 3d–f are**
 331 **the same as Figs. 3a–c, but the averaged surface temperature anomalies are only calculated within the global land regions. The**
 332 **trends of the fitting curves in K decade^{-1} are also presented in the legends.**



333

334 **Figure 4: Figures 4 (a) and (b) show monthly time-series data of global mean lightning flash rate anomalies with 1-D Gaussian**
 335 **(Denosing) Filter applied and their fitting curves of different experiments simulated respectively using the ECMWF-McCAUL**
 336 **scheme and CTH scheme. Figures 4 (c) and (d) are the same as Figs. 4 (a) and (b), except that the averaged lightning flash rate**
 337 **anomalies are calculated only within global land regions. Trends of the fitting curves (% yr⁻¹) are also shown in the legends.**

338

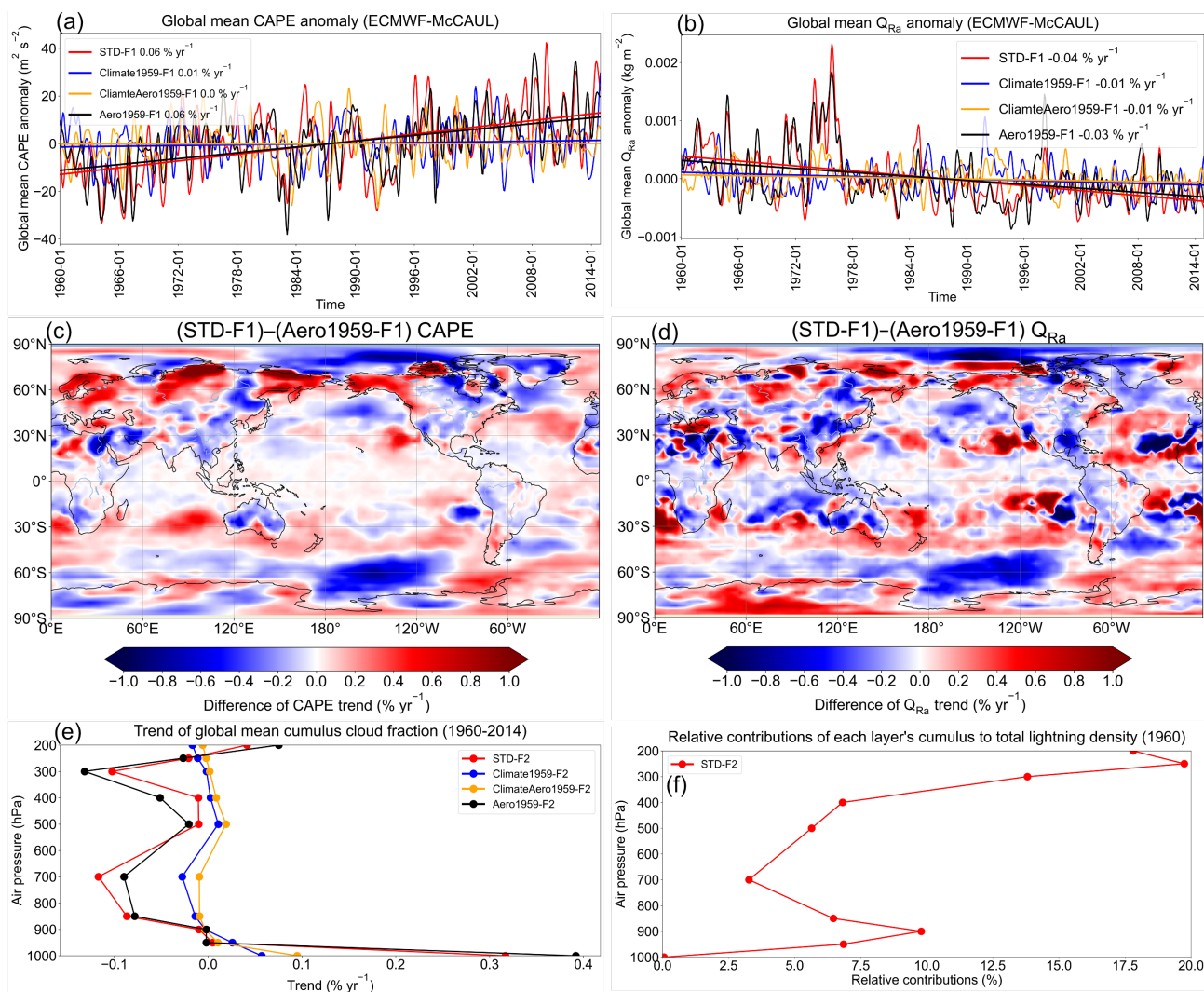
339 Figures 4 (a) and (b) respectively show the global mean lightning flash rate anomalies and their fitting curves obtained from
 340 the outputs of the ECMWF-McCAUL scheme and CTH scheme. The global lightning trend obtained from the STD-F1
 341 experiment turned out to be statistically flat (0.0% yr⁻¹), whereas the outputs of the STD-F2 experiment exhibit a not
 342 significant increasing global lightning trend (0.03% yr⁻¹) determined using the Mann–Kendall rank statistic (significance
 343 inferred for 5%).

344

345 From comparison of the lightning trends calculated from the STD and Climate1959 experiments, we found that both
 346 lightning schemes demonstrated that the historical global warming (1960–2014) enhances the global lightning trends toward
 347 positive trends (around 0.03% yr⁻¹ or 3% K⁻¹). The effects of global warming on historical lightning trends are evaluated as
 348 significant when using the CTH scheme, but not in the case of the ECMWF-McCAUL scheme. The differences in lightning
 349 trends simulated by the STD-F1/F2 and Aero1959-F1/F2 experiments indicate that the increases in AeroPEs during 1960–
 350 2014 significantly suppress the global lightning trends (-0.07% yr⁻¹ – -0.04% yr⁻¹). It is noteworthy that this suppression of
 351 lightning trends is only attributable to the aerosol radiative effects. Further research is needed to elucidate the long-term
 352 effects of aerosol on lightning through aerosol microphysical effects. We also investigated lightning trends only over land
 353 regions (Figs. 4c–d) to ascertain the effects of changes in AeroPEs to the greatest extent possible. When observing the



354 lightning trends over land only, the degree of suppression of lightning trends by increases in AeroPEs expands to $-0.10\% \text{ yr}^{-1}$
 355 $-0.05\% \text{ yr}^{-1}$, which is attributable to most AeroPEs and their growth coming from land regions. It is noteworthy that we
 356 used the same SSTs/sea ice data in the Aero1959 as those used for STD experiments. The SSTs/sea ice data also reflected
 357 the effects of increases in AeroPEs. Therefore, we might underestimate the effects of increases in AeroPEs on lightning
 358 trends by comparing the results of STD and Aero1959 experiments.



359
 360 **Figure 5:** Figures 5 (a) and (b) respectively show monthly time-series data of global mean CAPE and Q_{Ra}
 361 **Gaussian (Denoising) Filter** applied and their fitting curves simulated using the ECMWF-McCAUL scheme. Figures 5 (c) and (d),
 362 respectively show differences in the CAPE trend and Q_{Ra} trend of the STD-F1 and Aero1959-F1 experiments in the global map.
 363 **Figure 5e** portrays the vertical profiles of the global mean cumulus cloud fraction trend simulated by the CTH scheme. **Figure 5f**
 364 depicts the relative contributions of each layer's cumulus to total lightning density in 1960, as calculated from the outputs of the
 365 **STD-F2** experiment.



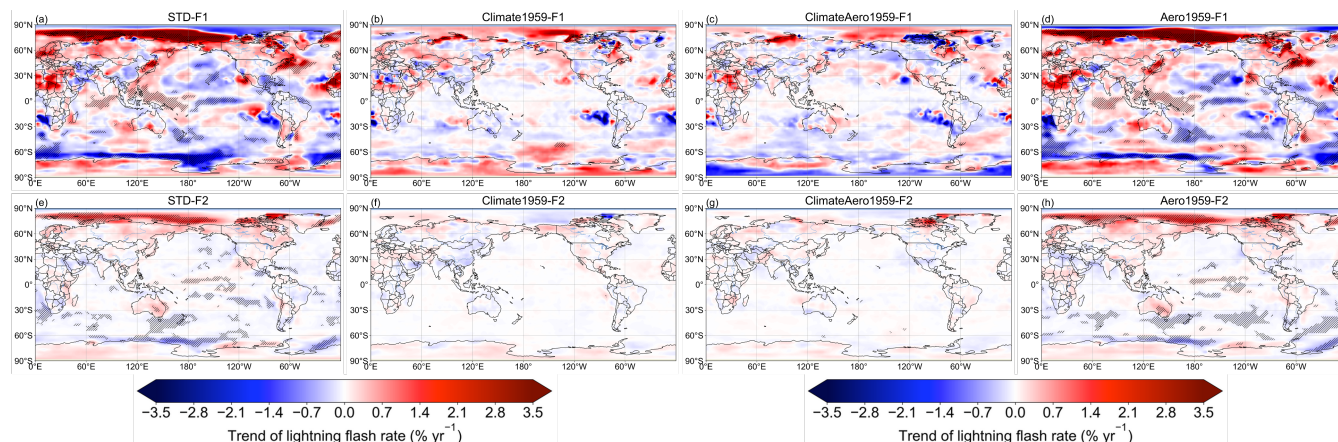
366

367 For the ECMWF-McCAUL scheme, model outputs affirm that global warming can enhance the global mean CAPE anomaly
368 slightly and suppress the global mean Q_{Ra} anomaly (Figs. 5a–b). The trend of the global mean Q_{Ra} anomaly can be
369 suppressed by earlier global warming, probably because global warming engenders the shifting of the $0^{\circ}\text{C} - -25^{\circ}\text{C}$ isotherm
370 to the higher region. Because global warming enhances global convection activities, and because lightning formation is
371 highly related to convection activity, global warming enhances the historical global lightning trend simulated by the
372 ECMWF-McCAUL scheme mainly as a result of the simulated CAPE trend, which is enhanced by global warming. The past
373 increases in AeroPEs exert negligible effects on the trends of global mean CAPE and Q_{Ra} anomalies, as displayed in Figs.
374 5a–b. However, the past increases in AeroPEs suppress the CAPE and Q_{Ra} trend within the tropical and subtropical terrestrial
375 regions where lightning densities are high (Figs. 5c–d). Weaker convection activities (smaller CAPE) and fewer
376 hydrometeors (cloud ice, graupel, snow) in the charge separation regions ($0^{\circ}\text{C} - -25^{\circ}\text{C}$ isotherm) lead to less lightning.
377 These are the main causes for the suppression of the historical lightning trends induced by increases in AeroPEs through
378 aerosol radiative effects.

379

380 To explain the results simulated by the CTH scheme, we investigated the vertical profiles of the trend of the global mean
381 cumulus cloud fraction (Fig. 5e). This is reasonable because each model layer's cumulus cloud fractions are used to weight
382 the calculated lightning densities from that layer in the CTH scheme, as introduced in equations (3) and (4). Figure 5f shows
383 the relative contributions of each model layer's cumulus to the calculated global total lightning densities in 1960 by the CTH
384 scheme. Cumulus convection is positively correlated with lightning formation, which is the scientific basis of parameterizing
385 lightning densities using the cumulus cloud top height: the CTH scheme. The historical global warming enhances the
386 lightning trend simulated by the CTH scheme mainly because the simulated historical global warming increases the cumulus
387 reaching 200 hPa, which contribute greatly to the simulated global total lightning density (Figs. 5e–f). The increases in the
388 deep convective cloud are regarded as related to the increases in tropopause height attributable to global warming, which is
389 shown in Fig. S1. The past increases in AeroPEs suppress the lightning trend simulated by the CTH scheme because
390 increases in AeroPEs decrease the cumulus reaching 200 hPa as well as the cumulus within the lower to middle troposphere
391 (Fig. 5f). Also, in the supplement we present a figure (Fig. S2) resembling Fig. 5, but which includes only consideration of
392 land regions. The mechanisms of global warming and increases in AeroPEs affecting lightning trends over land regions are
393 similar to those described above on a global scale. We do not discuss them in detail here.

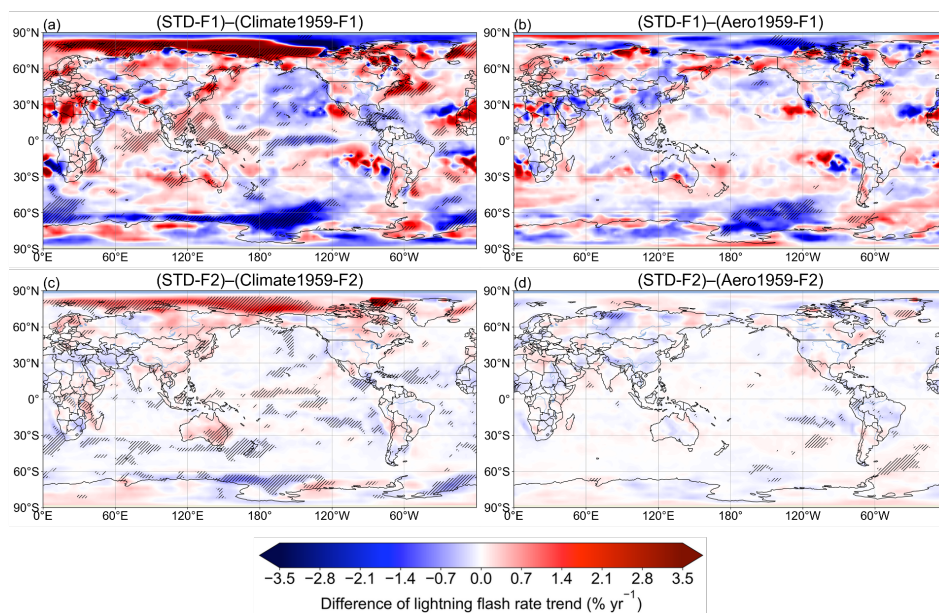
394



395

396 **Figure 6: Lightning flash rate trends ($\% \text{ yr}^{-1}$) during 1960–2014 on the two-dimensional map. The trend at every point was**
 397 **calculated from the function of approximating curve for the 1960–2014 time-series data at each grid cell. The area in which the**
 398 **trend was found to be significant by the Mann–Kendall rank statistic test (significance level inferred for 5%) is marked with**
 399 **hatched lines.**

400



401

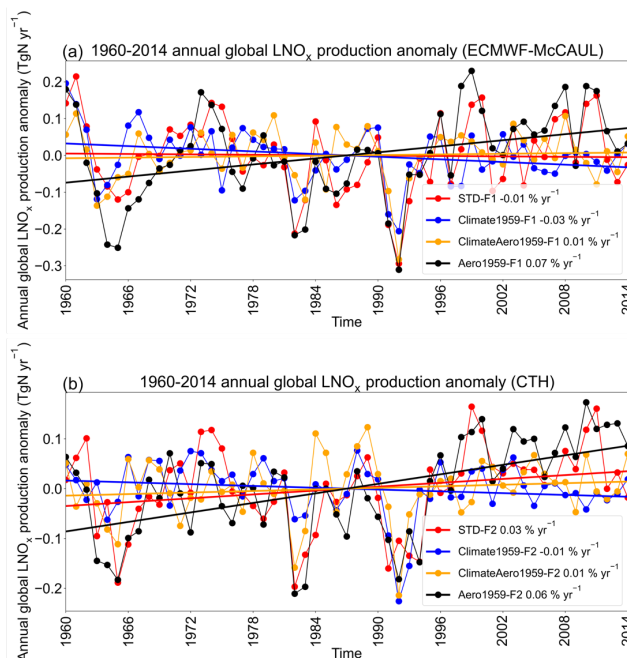
402 **Figure 7: Differences in lightning flash rate trends during 1960–2014 on the global map. The area in which the trend of the**
 403 **differences of lightning flash rate time-series data was found to be significant by the Mann–Kendall rank statistic test (significance**
 404 **level inferred for 5%) is marked with hatched lines.**

405

406 We also investigated lightning trends simulated from different experiments with the global map (Fig. 6). Both the ECMWF-
 407 McCAUL and the CTH schemes show that the lightning increased significantly in most parts of the Arctic region and



408 decreased in some parts of the Southern Ocean during 1960–2014 (Figs. 6a, e). The significant lightning trends presented in
 409 Figs. 6a almost disappeared when the climate simulations were fixed to 1959 (Figs. 6b, f), indicating the considerable effects
 410 of global warming on the trend of global lightning activities. Furthermore, the effects of past global warming and increases
 411 in AeroPEs on the lightning trends on the global map are displayed in Fig. 7. Figures 7a, c indicate that past global warming
 412 enhances lightning activities within the Arctic region and Japan, which is consistent with an earlier study from which Japan
 413 thunder day data were reported (Fujibe, 2017). Figures 7a, c also show that historical global warming suppresses lightning
 414 activities around New Zealand and some parts of the Southern Ocean. Both lightning schemes demonstrated that the
 415 historical increases in AeroPEs suppress lightning activities in some parts of the Southern Ocean and South America. The
 416 ECMWF-McCAUL scheme also suggests that historical increases in AeroPEs suppress lightning activities in some parts of
 417 India and China, where AeroPEs increased dramatically during 1960–2014 because of rapid economic development and
 418 energy consumption. We further provided the same figures as Figs. 6 and 7, but using different units ($\text{fl. km}^{-2} \text{ yr}^{-2}$) in the
 419 supplement (Figs. S3 and S4). Figures S3 and S4 show that the absolute lightning trends ($\text{fl. km}^{-2} \text{ yr}^{-2}$) and the effects of
 420 global warming and increases in AeroPEs on the absolute lightning trends are slight in high latitude regions.



421
 422 **Figure 8: Time-series data of 1960–2014 annual global LNO_x production anomalies (TgN yr^{-1}) and their fitting curves simulated**
 423 **using the ECMWF-McCAUL scheme (a) and the CTH scheme (b). Trends of the fitting curves in percent per year are shown in the**
 424 **legends.**

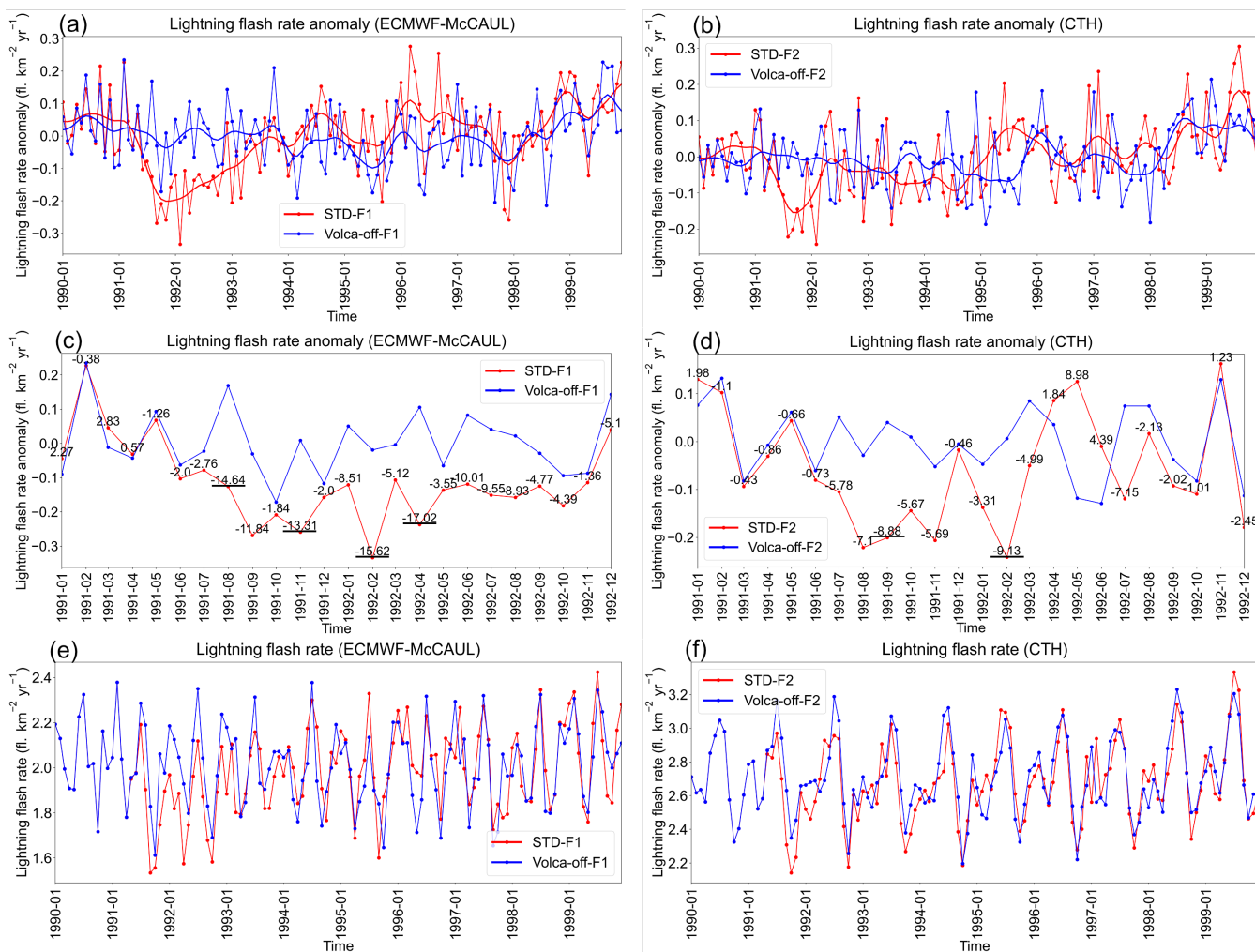
425
 426 Trends in historical annual global LNO_x emissions for different scenarios are generally consistent with trends in historical
 427 global mean lightning flash rates, as shown in Figs. 4a–b and Fig. 8. This finding is not surprising because, as the lightning
 428 NO_x emission parameterizations introduced in Sect. 2.2, the simulated lightning flash rates are linearly related to the



429 simulated LNO_x emissions in our study. The results presented in Fig. 8 imply that historical global warming and increases in
 430 AeroPEs can affect atmospheric chemistry and engender feedback by influencing LNO_x emissions.

431 **3.3 Effects of Pinatubo volcanic eruption on historical lightning–LNO_x trends**

432 We estimate the effects of the Pinatubo eruption on historical lightning–LNO_x trends and variation by comparing the
 433 simulation results of STD and Volca-off experiments. The simulated global mean lightning flash rates by STD and Volca-off
 434 experiments are the same until April 1991. They then begin to show differences from May 1991 (Figs. 9e–f). This is
 435 reasonable because the Pinatubo volcanic perturbations are removed from SAC during June 1991 through May 1994 in the
 436 Volca-off experiments by equation (11), and because the SAC of May 1991 used in CHASER are interpolated between the
 437 SAC of April 1991 and June 1991.



438
 439 **Figure 9: Time series of lightning flash rate or lightning flash rate anomalies from 1990 to 1999 or from 1991 through 1992.**
 440 **Figures 9(a–b) show the time series of lightning flash rate anomalies and their smoothed curves by 1-D Gaussian (Denosing) Filter**



441 from 1990 through 1999. Figures 9(c–d) present the time series of lightning flash rate anomalies from 1991 to 1992. The values
 442 shown over the red lines in Figs. 9(c–d) are *Relative_diff* calculated using equation 12. Figures 9(e–f) show the time series of
 443 lightning flash rate during 1990–1999.

444

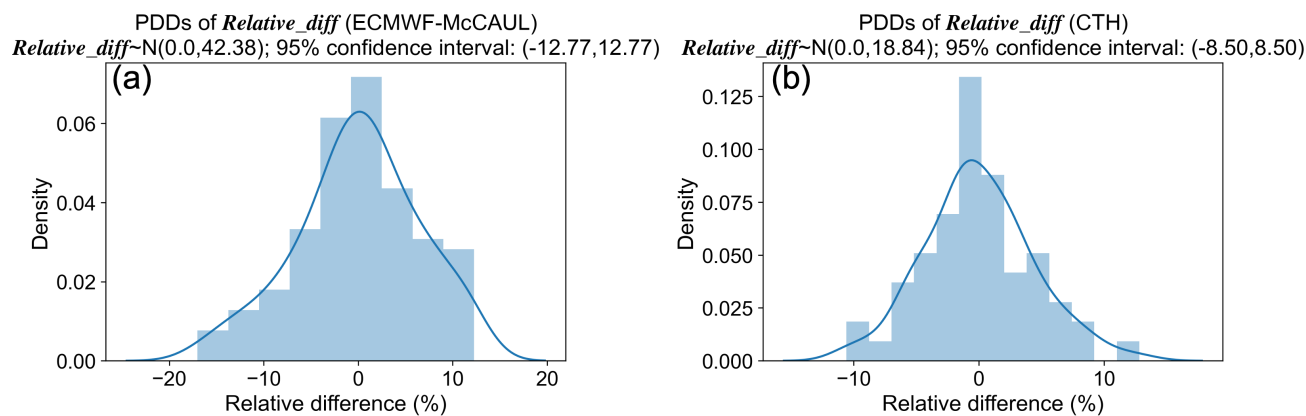
445 Figures 9c–d show the time series of lightning flash rate anomalies and *Relative_diff* (values over the red lines) from
 446 1991 to 1992. *Relative_diff* are relative differences of the global mean lightning flash rate anomalies between STD and
 447 Volca-off experiments calculated using the following equation.

448
$$\text{Relative_diff} = 100\% \times \frac{\text{LFRA}_{STD} - \text{LFRA}_{Volca-off}}{\text{LFR}_{Volca-off}} \quad (12)$$

449 In the equation, LFRA_{STD} represents global mean lightning flash rate anomalies simulated by STD-F1/F2 experiments.

450 $\text{LFRA}_{Volca-off}$ denotes global mean lightning flash rate anomalies simulated by Volca-off-F1/F2 experiments.

451 $\text{LFR}_{Volca-off}$ symbolizes global mean lightning flash rates simulated by Volca-off-F1/F2 experiments.

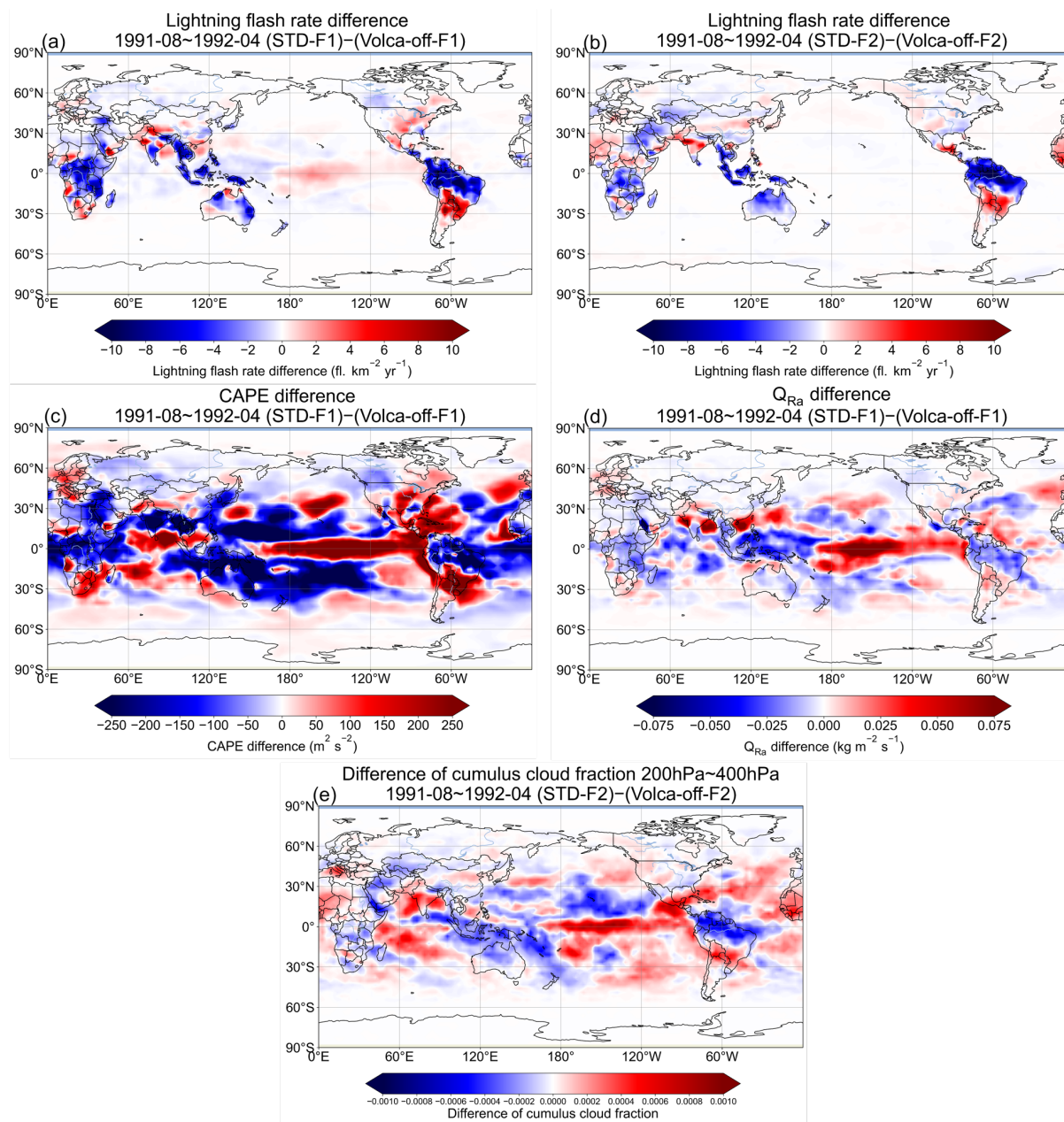


452

453 **Figure 10: Probability Density Distributions (PDDs) of *Relative_diff* obtained from monthly time-series data of *Relative_diff***
 454 **during 1990–1999. The 95% confidence interval of *Relative_diff* is also shown in the titles of this figure.**

455

456 The monthly time-series data of *Relative_diff* for 1990–1999 for both of the lightning schemes are calculated and the
 457 Probability Density Distributions (PDDs) of *Relative_diff* are displayed in Fig. 10. The *Relative_diff* presented in Fig.
 458 10 are all normally distributed as determined by the Kolmogorov–Smirnov test. The 95% confidence interval of
 459 *Relative_diff* is calculated and shown in the titles of Fig. 10. As displayed in Figs. 9c–d, the underlined values
 460 (*Relative_diff*) distributed within 1991-08 – 1992-04 outreached the 95% confidence interval, which means there are
 461 significant differences in calculated global mean lightning flash rate anomalies by STD and Volca-off experiments. In other
 462 words, global lightning activities were suppressed significantly by the Pinatubo eruption during the first year after the
 463 eruption.



464

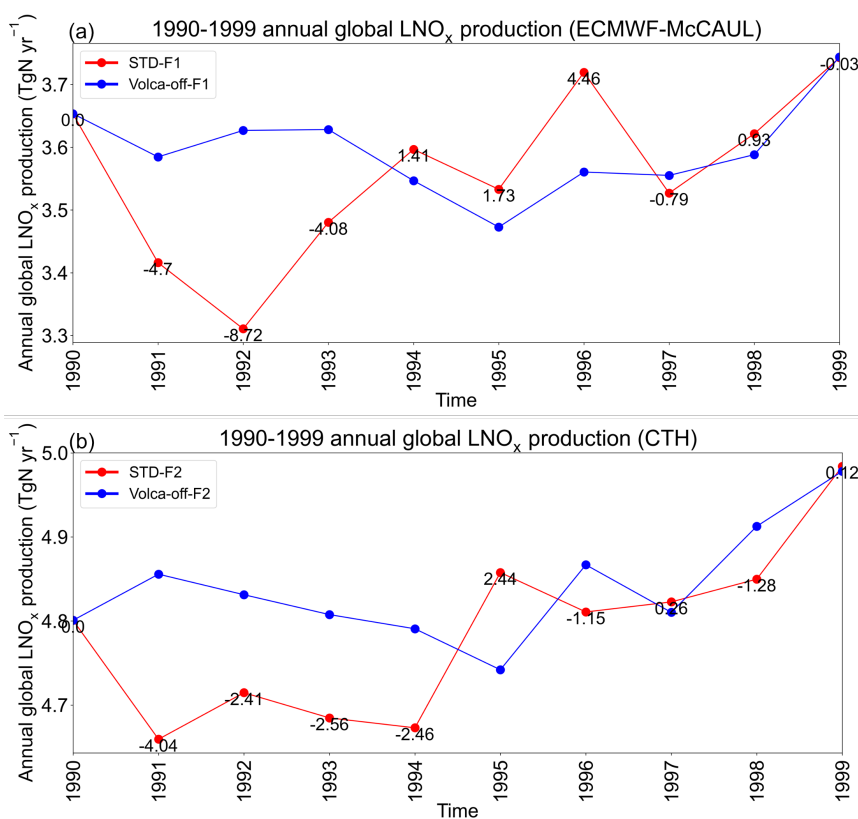
465 **Figure 11: 1991-08 – 1992-04 averaged lightning flash rate differences (a–b), CAPE differences (c), Q_{Ra} differences (d), and**
 466 **differences of 200 hPa – 400 hPa averaged cumulus cloud fraction (e) between STD and Volca-off experiments on the global map.**

467

468 Figures 11a–b show 1991-08 – 1992-04 averaged lightning flash rate differences between STD and Volca-off experiments
 469 on the global map. We found from Figs. 11a–b that lightning activities are suppressed significantly within the three hotspots
 470 of lightning activities (Central Africa, Maritime Continent, and South America) during 1991-08 – 1992-04 when the global



471 mean lightning flash rates are found to be suppressed. To explore the potential reasons for the suppressed global lightning
 472 activities in the first year after the Pinatubo eruption, we first investigated the 1991-08 – 1992-04 averaged CAPE and Q_{Ra}
 473 differences between STD-F1 and Volca-off-F1 (Figs. 11c–d) because lightning densities are computed with CAPE and Q_{Ra}
 474 by the ECMWF-McCAUL scheme. Results showed that the Pinatubo eruption can lead to apparent reductions of CAPE and
 475 Q_{Ra} within tropical and subtropical terrestrial regions (typically three hotspots of lightning activities) where lightning
 476 occurrence is frequent. These reductions constitute the main reason for the suppressed global lightning activities in the first
 477 year after the Pinatubo eruption simulated by the ECMWF-McCAUL scheme. We also examined the 1991-08 – 1992-04
 478 averaged differences of 200 hPa – 400 hPa averaged cumulus cloud fraction between STD-F2 and Volca-off-F2 on the
 479 global map (Fig. 11e). The cumulus cloud fractions of each model layer are used to weight the calculated lightning densities
 480 from that layer by the CTH scheme, as explained in Sect. 2.2. As depicted in Fig. 11e and Fig. S5, the Pinatubo eruption led
 481 to marked reductions in the middle to upper tropospheric cumulus cloud fractions during 1991-08 – 1992-04 over three
 482 hotspots of lightning activities (Central Africa, Maritime Continent, and South America). As displayed in Fig. 5f, the
 483 cumulus that reached the middle to upper troposphere is highly related to lightning formation. Consequently, the simulated
 484 global lightning activities by the CTH scheme were also suppressed considerably during the first year after the Pinatubo
 485 eruption.



486



487 **Figure 12: 1990–1999 annual global LNO_x emissions calculated from the STD and Volca-off experiments’ outputs simulated by the**
488 **ECMWF-McCAUL scheme (a) and the CTH scheme (b). Values over the red lines are the relative differences (%) between the red**
489 **lines and blue lines, calculated with respect to the blue lines.**

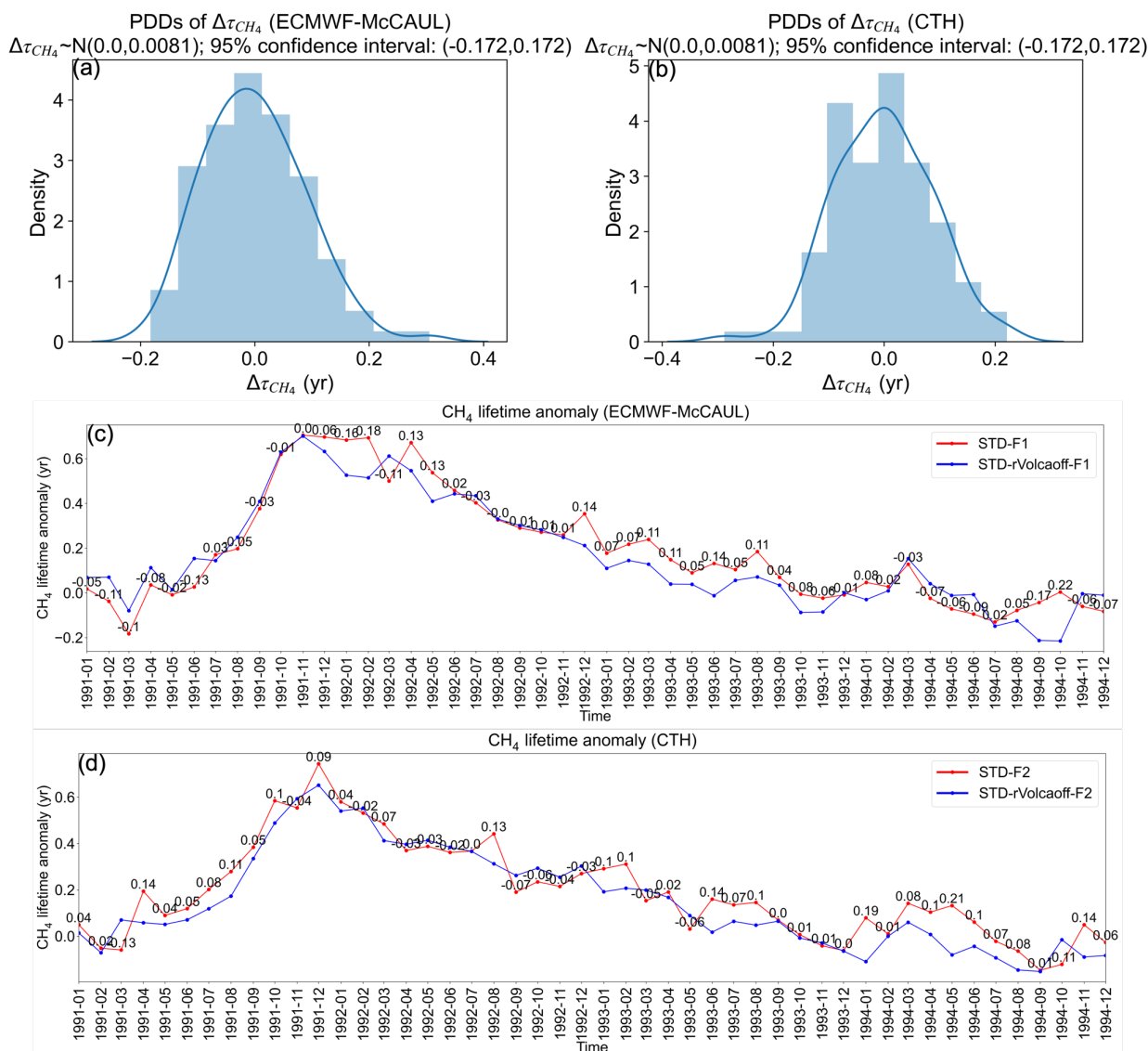
490

491 Aside from the previously described global lightning activity suppression, the production of LNO_x might also decrease after
492 the Pinatubo eruption. To explore this conjecture, we compared the LNO_x emissions in STD and Volca-off experiments (Fig.
493 12). In the case of the ECMWF-McCAUL scheme, the reduction of LNO_x emissions caused by the Pinatubo eruption started
494 in 1991 (4.70%) and continued until 1993, with the highest percentage reduction occurring in 1992 (8.72%) (Fig. 12a).
495 However, the CTH scheme showed a slightly different scenario of LNO_x emissions reduction after the Pinatubo eruption.
496 The LNO_x emissions are almost evenly reduced during 1991–1994 in the case of the CTH scheme (Fig. 12b). In conclusion,
497 our study indicates that the Pinatubo eruption can engender reductions in global LNO_x emissions, which last 2–3 years.
498 However, there exists some uncertainty in evaluating the magnitude of the reductions (from 2.41% to 8.72% for the annual
499 percentage reduction found from our study).

500

501 The simulated reduced global LNO_x emissions caused by the Pinatubo eruption might influence atmospheric chemistry
502 significantly. Most importantly, the reduced global LNO_x emissions might reduce OH radical production and extend the
503 global mean tropospheric lifetime of methane against tropospheric OH radical (hereinafter abbreviated as methane lifetime).
504 We investigated this point further by comparing the methane lifetime anomaly simulated by STD and STD-rVolcaoff
505 experiments. As introduced in Sect. 2.5, the settings of STD-rVolcaoff experiments are the same as those use for STD
506 experiments except for using the daily LNO_x emission rates calculated from the Volca-off experiments. We calculated the
507 monthly CH₄ lifetime anomalies during 1990–1999 and $\Delta\tau_{CH_4}$ (the difference of CH₄ lifetime anomaly between STD and
508 STD-rVolcaoff experiments), which are shown in Figs. 13c–d. Figures 13a–b display the PDDs of $\Delta\tau_{CH_4}$ monthly time series
509 during 1990–1999. The $\Delta\tau_{CH_4}$ shown in Figs. 13a–b are all normally distributed, as determined by the Kolmogorov–Smirnov
510 test. The 95% confidence interval of $\Delta\tau_{CH_4}$ is calculated and shown in the titles of Figs. 13a–b. The annual global LNO_x
511 production averaged during 1990–1999 is 3.56 TgN yr⁻¹ for STD-F1 and 4.79 TgN yr⁻¹ for STD-F2. At this level of annual
512 global LNO_x production, we found that within the first two years after the Pinatubo eruption, the $\Delta\tau_{CH_4}$ only slightly
513 outreached the 95% confidence interval in 1992-02 (0.18 years) simulated by the ECMWF-McCAUL scheme. However, the
514 widely cited range of annual global LNO_x production is 2–8 TgN yr⁻¹ (Schumann and Huntrieser, 2007). Presuming that
515 $\Delta\tau_{CH_4}$ linearly responds to the LNO_x emission level, and that the annual global LNO_x production is 8 TgN yr⁻¹, then the
516 extension of CH₄ lifetime because of the reduced LNO_x emissions can reach around 0.4 years for the ECMWF-McCAUL
517 scheme. As a comparison, ultraviolet shielding effects caused by stratospheric aerosols after the Pinatubo eruption led to the
518 maximum increase of the methane lifetime by about 0.6 years (Figs. 13c–d).

519



520

521 **Figure 13: (a–b) Probability Density Distributions (PDDs) of $\Delta\tau_{CH_4}$ obtained from the monthly time series data of $\Delta\tau_{CH_4}$ during**
 522 **$\Delta\tau_{CH_4}$ is the difference in CH₄ lifetime anomaly between STD and STD-rVolcaoff experiments. The 95% confidence**
 523 **interval of $\Delta\tau_{CH_4}$ is also presented in the titles of Figs. 13a–b. (c–d) Monthly time series of CH₄ lifetime anomalies simulated by**
 524 **STD-F1/F2 and STD-rVolcaoff-F1/F2 experiments. Values over the red lines are the difference in CH₄ lifetime anomaly between**
 525 **STD and STD-rVolcaoff experiments ($\Delta\tau_{CH_4}$).**

526



527 3.4 Model intercomparisons of lightning flash rate trends with CMIP6 model outputs

528 The historical lightning trends demonstrated in our study are undoubtedly worth comparing with the results of other
529 chemistry–climate models or Earth system models. As introduced in Sect. 2.4, for comparison of the simulated lightning
530 flash rate trends and variations in our study with those of other CMIP6 models’ outputs, we used all available lightning flash
531 rate data from the CMIP6 CMIP Historical experiments from CESM2-WACCM (3 ensembles) (Danabasoglu, 2019), GISS-
532 E2-1-G (9 ensembles) (Kelley et al., 2020), and UKESM1-0-LL (18 ensembles) (Tang et al., 2019). Please refer to Table S1
533 for the complete list of the ensemble members which were used. It is noteworthy that the lightning flash rate data obtained
534 from the three previously described CMIP6 models are calculated using the CTH scheme. The results of model
535 intercomparisons of lightning flash rate trends and variations are displayed in Fig. 14. As illustrated in Figs. 14a–b, both the
536 ECMWF-McCAUL and the CTH schemes (STD-F1/F2) simulated almost flat statistically non-significant global lightning
537 trends, but the ensemble mean obtained from another three CMIP6 models exhibit significant increasing global lightning
538 trends (trends from 0.11% yr⁻¹ to 0.25% yr⁻¹). Many reasons are responsible for the differences in global lightning trends
539 simulated by CHASER in our study and by the three CMIP6 models, including the use of different methods to determine
540 SSTs/sea ice fields. Instead of using a coupled Atmosphere–Ocean general circulation model to calculate SSTs/sea ice fields
541 dynamically in the three CMIP6 models, CHASER uses the prescribed HadISST data (Rayner et al., 2003), which are based
542 on plenty of observational data. Changes in global mean sea surface temperature during 1960–2014 (Δ SST) obtained from
543 STD-F1/F2 and CMIP6 model outputs are shown in Table 2. We also used the observation-based Extended Reconstructed
544 SST (ERSST) dataset (Huang et al., 2017) constructed by NOAA to evaluate the Δ SST obtained from different models. The
545 Δ SST calculated from ERSST during 1960–2014 is 0.543°C, which is most close to the Δ SST obtained from STD-F1/F2.
546 Considered from the perspective of SSTs/sea ice fields alone, the results (global lightning trends) of our study are expected
547 to be closer to the actual situation.

548

549 Actually, the three CMIP6 models simulated stronger global warming during 1960–2014 than CHASER in our study, as
550 displayed in Fig. S6. The CTH scheme is reported to respond positively to simulated global warming (Price and Rind, 1994;
551 Zeng et al., 2008; Hui and Hong, 2013; Banerjee et al., 2014; Krause et al., 2014; Clark et al., 2017). The simulated stronger
552 global warming by the three CMIP6 models is regarded as responsible for differences in simulated global lightning trends
553 between our study and the three CMIP6 models (Figs. 14a–b). We further investigated the sensitivities of the global mean
554 lightning flash rate change to the global mean surface temperature increase (% °C⁻¹) obtained from CHASER and the three
555 CMIP6 models. The sensitivities in percentage per degree Celsius are presented in Table 2. Overall, even when using the
556 same CTH scheme, the sensitivities (Δ LFR/ Δ TS) simulated by the three CMIP6 models are higher than that simulated by
557 CHASER in our study. This might be partially attributable to the nonlinear relation between lightning response and climate
558 change (Pinto, 2013; Krause et al., 2014). Compared to the CTH scheme, the ECMWF-McCAUL scheme simulated a



559 statistically non-significant negative sensitivity ($\Delta\text{LFR}/\Delta\text{TS}$), which is attributable to the stronger suppression of positive
560 global lightning trends caused by increases in AeroPEs simulated by the ECMWF-McCAUL scheme.

561

562 **Table 2: Changes in global mean surface temperature (ΔTS), global mean sea surface temperature (ΔSST), global mean lightning**
563 **flash rate (ΔLFR), and the rate of change of lightning flash rate corresponding to each degree Celsius increase in global mean**
564 **surface temperature ($\Delta\text{LFR}/\Delta\text{TS}$) obtained from STD-F1/F2 and CMIP6 model outputs. Changes were obtained by calculating the**
565 **difference between the rightmost and leftmost points of the approximating curve for the 1960–2014 time-series data.**

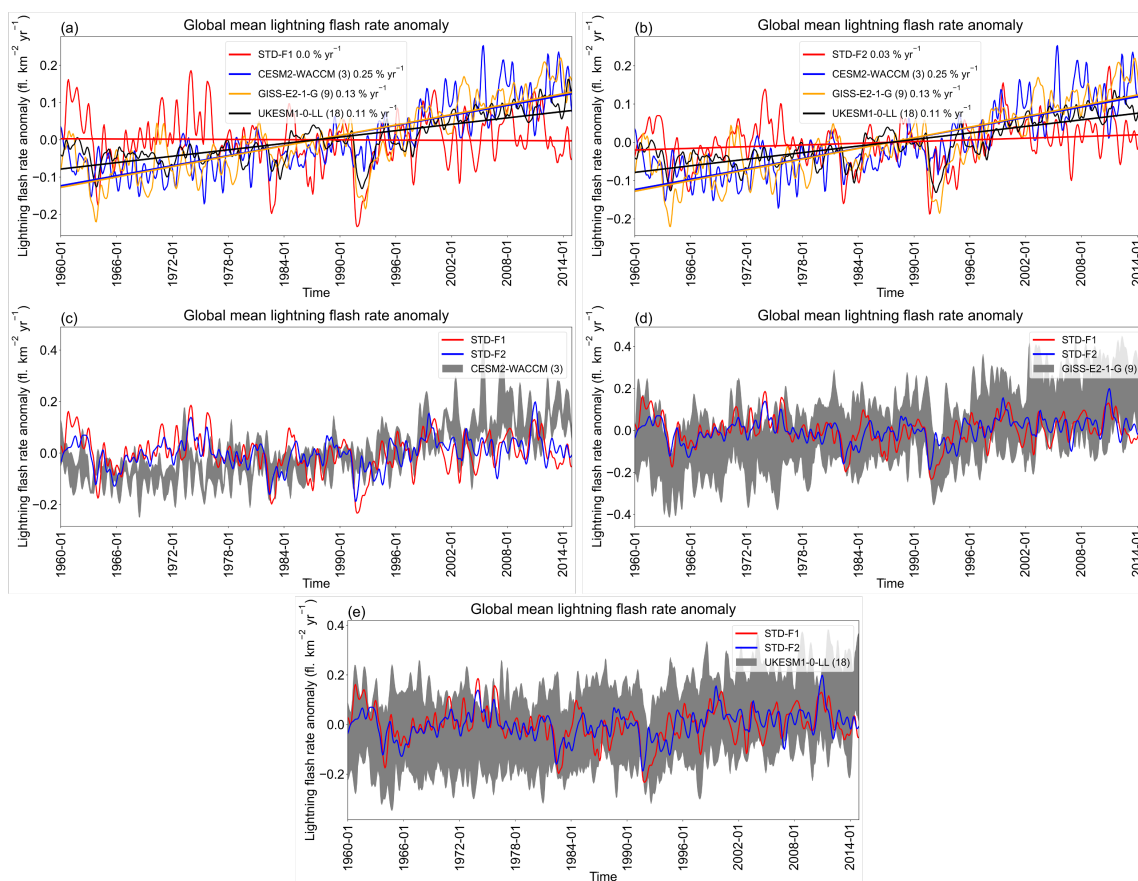
Model/experiment/dataset	ΔTS ($^{\circ}\text{C}$)	ΔSST ($^{\circ}\text{C}$)	ΔLFR (%)	$\Delta\text{LFR}/\Delta\text{TS}$ ($\% \text{ } ^{\circ}\text{C}^{-1}$)
STD-F1	0.615	0.425	-0.374	-0.61
STD-F2	0.585	0.432	1.376	2.35
CESM2-WACCM	1.266	1.074	13.780	10.88
GISS-E2-1-G	0.823	0.668	7.079	8.60
UKESM1-0-LL	1.167	1.004	5.791	5.43
ERSST	—	0.543	—	—

566

567 Figures 14d–e affirm that the global lightning variation simulated by our study is basically within the full ensemble range of
568 GISS-E2-1-G and UKESM1-0-LL. After the Pinatubo eruption, as described in Sect. 3.3 of this report, the GISS-E2-1-G and
569 UKESM1-0-LL models also manifest significant suppression of global lightning activities, but the CESM2-WACCM model
570 does not show this phenomenon. The commonalities as well as differences in global lightning trends and variations found in



571 the model intercomparisons imply that great uncertainties existed in past (1960–2014) global lightning trend simulations.
 572 Such uncertainties deserve to be investigated further.



573
 574 **Figure 14: Comparisons of simulated global mean lightning flash rate anomalies found in our study (CHASER) and other CMIP6**
 575 **models. All the figures are created based on the monthly time-series data of global mean lightning flash rate anomalies with a 1-D**
 576 **Gaussian (Denoising) Filter applied. For CMIP6 models, the ensemble mean is shown as the solid line; the full ensemble range is**
 577 **shown as grey shading (c–e). Fitting curves and the trends of fitting curves (% yr⁻¹) are also given in (a–b).**

578 4 Discussions and Conclusions

579 We used two lightning schemes (the CTH and ECMWF-McCAUL schemes) to study historical (1960–2014) lightning–
 580 LNO_x trends and variations and their controlling factors (global warming, increases in AeroPEs, and Pinatubo eruption)
 581 within the CHASER (MIROC) chemistry–climate model. The CTH scheme is the most widely used lightning scheme, but it
 582 lacks a direct physical link with the charging mechanism. The ECMWF-McCAUL scheme is a newly developed process-
 583 based/ice-based lightning scheme with a direct physical link to the charging mechanism.

584



585 With only the aerosol radiative effects considered in the lightning–aerosols interaction, both lightning schemes simulated
586 almost flat trends of global mean lightning flash rate during 1960–2014. Reportedly, because the aerosol microphysical
587 effects can enhance lightning activities (Yuan et al., 2011; Wang et al., 2018; Liu et al., 2020), our study might
588 underestimate the increasing trend of global mean lightning flash rate (our study only considered the aerosol radiative effects
589 in aerosol–lightning interactions). Further research is expected considering the effects of aerosol microphysical effects on
590 long-term lightning trends. Moreover, both lightning schemes manifest that past global warming enhances the historical
591 trend of global mean lightning density toward the positive direction (around $0.03\% \text{ yr}^{-1}$ or $3\% \text{ K}^{-1}$). However, past increases
592 in AeroPEs exert the opposite effect to the lightning trend ($-0.07\% \text{ yr}^{-1}$ – $-0.04\% \text{ yr}^{-1}$). The effects of the increases in
593 AeroPEs on the lightning trend only over land regions expand to $-0.10\% \text{ yr}^{-1}$ – $-0.05\% \text{ yr}^{-1}$, which implies that the effects are
594 more significant over land regions. We obtained similar results for the historical global LNO_x emissions trend, which
595 indicates that historical global warming and increases in AeroPEs can affect atmospheric chemistry and engender feedback
596 by influencing LNO_x emissions. Although the CTH and ECMWF-McCAUL schemes use different parameters to simulate
597 lightning, both lightning schemes indicate that the enhanced global convective activity under global warming is the main
598 reason for the increase in lightning– LNO_x emissions. In contrast, the increases in AeroPEs have decreased lightning– LNO_x
599 emissions by weakening convective activity in the hotspots of lightning. By analyzing the simulation results on the global
600 map, we also found that the effects of historical global warming and increases in AeroPEs on lightning trends are
601 heterogeneous across different regions. Our results indicate that historical global warming enhances lightning activities
602 within the Arctic region and Japan but suppresses lightning activities around New Zealand and some parts of the Southern
603 Ocean. Both lightning schemes demonstrated that the historical increases in AeroPEs suppress lightning activities in some
604 parts of the Southern Ocean and South America. The ECMWF-McCAUL scheme also suggests that historical increases in
605 AeroPEs suppress lightning activities in some parts of India and China. This finding is plausible because both countries
606 experienced dramatic increases in AeroPEs during 1960–2014 because of rapid economic growth.

607

608 Furthermore, this report is the first describing that global lightning activity was suppressed significantly during the first year
609 after the Pinatubo eruption, which is indicated in both lightning schemes (global lightning activities decreased by up to
610 17.02% simulated by the ECMWF-McCAUL scheme). This finding is mainly attributable to the Pinatubo eruption
611 weakening of the convective activities within the hotspots of lightning, which in turn decreased the amount of column
612 precipitating ice (Q_{Ra}) and middle-level to high-level cumulus cloud fractions in these regions. The simulation results also
613 indicate that the Pinatubo eruption can engender reductions in global LNO_x emissions, which last 2–3 years. However, some
614 uncertainty exists in evaluating magnitude of these reductions (from 2.41% to 8.72% for the annual percentage reduction in
615 our study). The case study of the Pinatubo eruption in our research indicates that other large-scale volcanic eruptions can
616 also engender significant reduction of global lightning activities and global-scale LNO_x emissions.

617



618 Lastly, we compared the global lightning trends demonstrated in our study with the outputs of three CMIP6 models:
619 CESM2-WACCM, GISS-E2-1-G, and UKESM1-0-LL. We used all available lightning flash rate data from the CMIP6
620 CMIP historical experiments from the three models described above. The three CMIP6 models suggested significant
621 increasing trends in historical global lightning activities, which differs from the findings of our study. Unlike the three
622 CMIP6 models that use a coupled Atmosphere–Ocean general circulation model to calculate SSTs/sea ice fields dynamically,
623 our study (CHASER) uses the prescribed HadISST SSTs/sea ice data which are closer to the actual situation. Therefore, we
624 believe that the results (the historical global lightning trends) obtained from our study (CHASER) are closer to the actual
625 situation. However, model intercomparisons of global lightning trends still indicate that significant uncertainties exist in the
626 historical (1960–2014) global lightning trend simulations, and that such uncertainties deserve further investigation.

627 **Code availability**

628 The source code for CHASER to reproduce results obtained from this work is obtainable from the repository at
629 <https://doi.org/10.5281/zenodo.5835796> (He et al., 2022a).

630 **Data availability**

631 The LIS/OTD data used for this study are available from <https://ghrc.nsstc.nasa.gov/hydro/?q=LRTS> (last access: 11 January
632 2022). The CMIP6 model outputs (lightning flash rate and surface temperature) used for this study are available from
633 <https://aims2.llnl.gov/search> (last access: 1 February 2023). The Extended Reconstructed SST data used for this study are
634 available from <https://www.ncei.noaa.gov/products/extended-reconstructed-sst> (last access: 27 March 27 2023).

635 **Author contribution**

636 YFH conducted all simulations, interpreted the results, and wrote the manuscript. KS developed the CHASER (MIROC)
637 model code, conceived the presented idea, and supervised the findings of this work and the manuscript preparation.

638 **Competing interests**

639 The authors declare that they have no conflict of interest.

640 **Acknowledgments**

641 This research was supported by the Global Environment Research Fund (S–12 and S–20) of the Ministry of the Environment
642 (MOE), Japan, and JSPS KAKENHI Grant Numbers: JP20H04320, JP19H05669, and JP19H04235. This work was



643 supported by the Japan Science and Technology Agency (JST) Support for Pioneering Research Initiated by the Next
644 Generation (SPRAINING), Grant Number JPMJSP2125. The author would like to take this opportunity to thank the
645 “Interdisciplinary Frontier Next-Generation Researcher Program of the Tokai Higher Education and Research System.” The
646 simulations were completed with the supercomputer (NEC SX-Aurora TSUBASA) at NIES (Japan). We thank NASA
647 scientists and staff for providing LIS/OTD lightning observation data. We acknowledge the World Climate Research
648 Programme, which coordinated and promoted CMIP6 through its Working Group on Coupled Modelling. We extend our
649 sincere gratitude to the climate modelling groups for producing and providing their model outputs, to the Earth System Grid
650 Federation (ESGF) for archiving the data and providing free downloads, and to the multiple funding agencies that have
651 supported the CMIP6 as well as the Earth System Grid Federation. We also thank Ms. Do Thi Nhu Ngoc for her assistance in
652 downloading the CMIP6 model outputs.

653 References

- 654 Allen, D. J., Pickering, K. E., Bucsela, E., Krotkov, N., and Holzworth, R.: Lightning NO_x Production in the Tropics as
655 Determined Using OMI NO₂ Retrievals and WLLN Stroke Data, *Journal of Geophysical Research: Atmospheres*,
656 124, 13498–13518, <https://doi.org/10.1029/2018JD029824>, 2019.
- 657 Altartz, O., Kucienska, B., Kostinski, A., Raga, G. B., and Koren, I.: Global association of aerosol with flash density of
658 intense lightning, *Environ. Res. Lett.*, 12, 114037, <https://doi.org/10.1088/1748-9326/aa922b>, 2017.
- 659 Earle Williams: <https://web.mit.edu/earlerw/www/index.html>, last access: 19 December 2022.
- 660 Climate at a Glance | National Centers for Environmental Information (NCEI):
661 https://www.ncei.noaa.gov/access/monitoring/climate-at-a-glance/global/time-series/globe/land_ocean/3/8/1880-2020,
662 last access: 23 October 2022.
- 663 Arfeuille, F., Luo, B. P., Heckendorn, P., Weisenstein, D., Sheng, J. X., Rozanov, E., Schraner, M., Brönnimann, S.,
664 Thomason, L. W., and Peter, T.: Modeling the stratospheric warming following the Mt. Pinatubo eruption:
665 uncertainties in aerosol extinctions, *Atmospheric Chemistry and Physics*, 13, 11221–11234,
666 <https://doi.org/10.5194/acp-13-11221-2013>, 2013.
- 667 Banerjee, A., Archibald, A. T., Maycock, A. C., Telford, P., Abraham, N. L., Yang, X., Braesicke, P., and Pyle, J. A.:
668 Lightning NO_x, a key chemistry-climate interaction: Impacts of future climate change and consequences for
669 tropospheric oxidising capacity, *Atmospheric Chemistry and Physics*, 14, 9871–9881, <https://doi.org/10.5194/acp-14-9871-2014>, 2014.
- 671 Boucher, O.: *Atmospheric Aerosols*, Springer Netherlands, Dordrecht, <https://doi.org/10.1007/978-94-017-9649-1>, 2015.
- 672 Bucsela, E. J., Pickering, K. E., Allen, D. J., Holzworth, R. H., and Krotkov, N. A.: Midlatitude Lightning NO_x Production
673 Efficiency Inferred From OMI and WLLN Data, *Journal of Geophysical Research: Atmospheres*, 124, 13475–
674 13497, <https://doi.org/10.1029/2019JD030561>, 2019.
- 675 Cecil, D. J., Buechler, D. E., and Blakeslee, R. J.: Gridded lightning climatology from TRMM-LIS and OTD: Dataset
676 description, *Atmospheric Research*, 135–136, 404–414, <https://doi.org/10.1016/j.atmosres.2012.06.028>, 2014.
- 677 Cerveny, R. S., Bessemoulin, P., Burt, C. C., Cooper, M. A., Cunjje, Z., Dewan, A., Finch, J., Holle, R. L., Kalkstein, L.,
678 Kruger, A., Lee, T., Martinez, R., Mohapatra, M., Pattanaik, D. R., Peterson, T. C., Sheridan, S., Trewin, B., Tait, A.,
679 and Wahab, M. M. A.: WMO Assessment of Weather and Climate Mortality Extremes: Lightning, Tropical Cyclones,
680 Tornadoes, and Hail, *Weather, Climate, and Society*, 9, 487–497, <https://doi.org/10.1175/WCAS-D-16-0120.1>, 2017.
- 681 Clark, S. K., Ward, D. S., and Mahowald, N. M.: Parameterization-based uncertainty in future lightning flash density,
682 *Geophysical Research Letters*, 44, 2893–2901, <https://doi.org/10.1002/2017GL073017>, 2017.



- 683 Cooper, M. A. and Holle, R. L.: Current Global Estimates of Lightning Fatalities and Injuries, in: *Reducing Lightning*
684 *Injuries Worldwide*, edited by: Cooper, M. A. and Holle, R. L., Springer International Publishing, Cham, 65–73,
685 https://doi.org/10.1007/978-3-319-77563-0_6, 2019.
- 686 Cooray, V., Rahman, M., and Rakov, V.: On the NO_x production by laboratory electrical discharges and lightning, *Journal of*
687 *Atmospheric and Solar-Terrestrial Physics*, 71, 1877–1889, <https://doi.org/10.1016/j.jastp.2009.07.009>, 2009.
- 688 Danabasoglu, G.: NCAR CESM2-WACCM model output prepared for CMIP6 CMIP historical,
689 <https://doi.org/10.22033/ESGF/CMIP6.10071>, 2019.
- 690 Danabasoglu, G., Lamarque, J.-F., Bacmeister, J., Bailey, D. A., DuVivier, A. K., Edwards, J., Emmons, L. K., Fasullo, J.,
691 Garcia, R., Gettelman, A., Hannay, C., Holland, M. M., Large, W. G., Lauritzen, P. H., Lawrence, D. M., Lenaerts, J.
692 T. M., Lindsay, K., Lipscomb, W. H., Mills, M. J., Neale, R., Oleson, K. W., Otto-Bliesner, B., Phillips, A. S., Sacks,
693 W., Tilmes, S., van Kampenhout, L., Vertenstein, M., Bertini, A., Dennis, J., Deser, C., Fischer, C., Fox-Kemper, B.,
694 Kay, J. E., Kinnison, D., Kushner, P. J., Larson, V. E., Long, M. C., Mickelson, S., Moore, J. K., Nienhouse, E.,
695 Polvani, L., Rasch, P. J., and Strand, W. G.: The Community Earth System Model Version 2 (CESM2), *Journal of*
696 *Advances in Modeling Earth Systems*, 12, e2019MS001916, <https://doi.org/10.1029/2019MS001916>, 2020.
- 697 Del Genio, A. D., Yao, M.-S., and Jonas, J.: Will moist convection be stronger in a warmer climate?, *Geophysical Research*
698 *Letters*, 34, <https://doi.org/10.1029/2007GL030525>, 2007.
- 699 Finney, D. L., Doherty, R. M., Wild, O., Huntrieser, H., Pumphrey, H. C., and Blyth, A. M.: Using cloud ice flux to
700 parametrise large-scale lightning, *Atmospheric Chemistry and Physics*, 14, 12665–12682,
701 <https://doi.org/10.5194/acp-14-12665-2014>, 2014.
- 702 Finney, D. L., Doherty, R. M., Wild, O., Young, P. J., and Butler, A.: Response of lightning NO_x emissions and ozone
703 production to climate change: Insights from the Atmospheric Chemistry and Climate Model Intercomparison Project,
704 *Geophysical Research Letters*, 43, 5492–5500, <https://doi.org/10.1002/2016GL068825>, 2016a.
- 705 Finney, D. L., Doherty, R. M., Wild, O., and Abraham, N. L.: The impact of lightning on tropospheric ozone chemistry using
706 a new global lightning parametrisation, *Atmospheric Chemistry and Physics*, 16, 7507–7522,
707 <https://doi.org/10.5194/acp-16-7507-2016>, 2016b.
- 708 Finney, D. L., Doherty, R. M., Wild, O., Stevenson, D. S., MacKenzie, I. A., and Blyth, A. M.: A projected decrease in
709 lightning under climate change, *Nature Climate Change*, 8, 210–213, <https://doi.org/10.1038/s41558-018-0072-6>,
710 2018.
- 711 Fujibe, F.: Long-term Change in Lightning Mortality and Its Relation to Annual Thunder Days in Japan, *Journal of Natural*
712 *Disaster Science*, 38, 17–29, <https://doi.org/10.2328/jnds.38.17>, 2017.
- 713 Goodman, S. J., Buechler, D. E., and Wright, P. D.: Lightning/rainfall relationships during COHMEX, NTRS Author
714 Affiliations: NASA Marshall Space Flight Center, Universities Space Research Association NTRS Document ID:
715 19900057799 NTRS Research Center: Legacy CDMS (CDMS), 1990.
- 716 Goto, D., Nakajima, T., Dai, T., Takemura, T., Kajino, M., Matsui, H., Takami, A., Hatakeyama, S., Sugimoto, N., Shimizu,
717 A., and Ohara, T.: An evaluation of simulated particulate sulfate over East Asia through global model
718 intercomparison, *Journal of Geophysical Research: Atmospheres*, 120, 6247–6270,
719 <https://doi.org/10.1002/2014JD021693>, 2015.
- 720 Guenther, A. B., Jiang, X., Heald, C. L., Sakulyanontvittaya, T., Duhl, T., Emmons, L. K., and Wang, X.: The Model of
721 Emissions of Gases and Aerosols from Nature version 2.1 (MEGAN2.1): an extended and updated framework for
722 modeling biogenic emissions, *Geosci. Model Dev.*, 5, 1471–1492, <https://doi.org/10.5194/gmd-5-1471-2012>, 2012.
- 723 Ha, P. T. M., Matsuda, R., Kanaya, Y., Taketani, F., and Sudo, K.: Effects of heterogeneous reactions on tropospheric
724 chemistry: A global simulation with the chemistry-climate model CHASER V4.0, *Geoscientific Model Development*,
725 14, 3813–3841, <https://doi.org/10.5194/gmd-14-3813-2021>, 2021.
- 726 He, Y., Hoque, M. S. H., and Sudo, K.: Introducing new lightning schemes into the CHASER (MIROC) chemistry climate
727 model [Code], Zenodo, <https://doi.org/10.5281/zenodo.5835796>, 2022a.
- 728 He, Y., Hoque, H. M. S., and Sudo, K.: Introducing new lightning schemes into the CHASER (MIROC) chemistry–climate
729 model, *Geoscientific Model Development*, 15, 5627–5650, <https://doi.org/10.5194/GMD-15-5627-2022>, 2022b.
- 730 Hoesly, R. M., Smith, S. J., Feng, L., Klimont, Z., Janssens-Maenhout, G., Pitkanen, T., Seibert, J. J., Vu, L., Andres, R. J.,
731 Bolt, R. M., Bond, T. C., Dawidowski, L., Kholod, N., Kurokawa, J., Li, M., Liu, L., Lu, Z., Moura, M. C. P.,
732 O'Rourke, P. R., and Zhang, Q.: Historical (1750–2014) anthropogenic emissions of reactive gases and aerosols from



- 733 the Community Emissions Data System (CEDS), *Geosci. Model Dev.*, 11, 369–408, [https://doi.org/10.5194/gmd-11-](https://doi.org/10.5194/gmd-11-369-2018)
734 369-2018, 2018.
- 735 Huang, B., Thorne, P. W., Banzon, V. F., Boyer, T., Chepurin, G., Lawrimore, J. H., Menne, M. J., Smith, T. M., Vose, R. S.,
736 and Zhang, H.-M.: Extended Reconstructed Sea Surface Temperature, Version 5 (ERSSTv5): Upgrades, Validations,
737 and Intercomparisons, *Journal of Climate*, 30, 8179–8205, <https://doi.org/10.1175/JCLI-D-16-0836.1>, 2017.
- 738 Hui, J. and Hong, L.: Projected Changes in NO_x Emissions from Lightning as a Result of 2000–2050 Climate Change,
739 *Atmospheric and Oceanic Science Letters*, 6, 284–289, <https://doi.org/10.3878/j.issn.1674-2834.13.0042>, 2013.
- 740 Ito, A. and Inatomi, M.: Water-use efficiency of the terrestrial biosphere: A model analysis focusing on interactions between
741 the global carbon and water cycles, *Journal of Hydrometeorology*, 13, 681–694, [https://doi.org/10.1175/JHM-D-10-](https://doi.org/10.1175/JHM-D-10-05034.1)
742 05034.1, 2012.
- 743 Jensen, J. D., Thurman, J., and Vincent, A. L.: *Lightning Injuries*, in: StatPearls, StatPearls Publishing, Treasure Island (FL),
744 2022.
- 745 Kaufman, Y. J., Tanré, D., Holben, B. N., Mattoo, S., Remer, L. A., Eck, T. F., Vaughan, J., and Chatenet, B.: Aerosol
746 Radiative Impact on Spectral Solar Flux at the Surface, Derived from Principal-Plane Sky Measurements, *Journal of*
747 *the Atmospheric Sciences*, 59, 635–646, [https://doi.org/10.1175/1520-0469\(2002\)059<0635:AROSS>2.0.CO;2](https://doi.org/10.1175/1520-0469(2002)059<0635:AROSS>2.0.CO;2),
748 2002.
- 749 Kelley, M., Schmidt, G. A., Nazarenko, L. S., Bauer, S. E., Ruedy, R., Russell, G. L., Ackerman, A. S., Aleinov, I., Bauer,
750 M., Bleck, R., Canuto, V., Cesana, G., Cheng, Y., Clune, T. L., Cook, B. I., Cruz, C. A., Del Genio, A. D., Elsaesser,
751 G. S., Faluvegi, G., Kiang, N. Y., Kim, D., Lacis, A. A., Leboissetier, A., LeGrande, A. N., Lo, K. K., Marshall, J.,
752 Matthews, E. E., McDermid, S., Mezzuman, K., Miller, R. L., Murray, L. T., Oinas, V., Orbe, C., García-Pando, C. P.,
753 Perlwitz, J. P., Puma, M. J., Rind, D., Romanou, A., Shindell, D. T., Sun, S., Tausnev, N., Tsigaridis, K., Tselioudis,
754 G., Weng, E., Wu, J., and Yao, M.-S.: GISS-E2.1: Configurations and Climatology, *Journal of Advances in Modeling*
755 *Earth Systems*, 12, e2019MS002025, <https://doi.org/10.1029/2019MS002025>, 2020.
- 756 Koren, I., Kaufman, Y. J., Remer, L. A., and Martins, J. V.: Measurement of the Effect of Amazon Smoke on Inhibition of
757 Cloud Formation, *Science*, 303, 1342–1345, <https://doi.org/10.1126/science.1089424>, 2004.
- 758 Koren, I., Martins, J. V., Remer, L. A., and Afargan, H.: Smoke Invigoration Versus Inhibition of Clouds over the Amazon,
759 *Science*, 321, 946–949, <https://doi.org/10.1126/science.1159185>, 2008.
- 760 Krause, A., Kloster, S., Wilkenskeld, S., and Paeth, H.: The sensitivity of global wildfires to simulated past, present, and
761 future lightning frequency, *Journal of Geophysical Research: Biogeosciences*, 119, 312–322,
762 <https://doi.org/10.1002/2013JG002502>, 2014.
- 763 Labrador, L. J., von Kuhlmann, R., and Lawrence, M. G.: The effects of lightning-produced NO_x and its vertical distribution
764 on atmospheric chemistry: sensitivity simulations with MATCH-MPIC, *Atmospheric Chemistry and Physics*, 5,
765 1815–1834, <https://doi.org/10.5194/acp-5-1815-2005>, 2005.
- 766 Li, Z., Guo, J., Ding, A., Liao, H., Liu, J., Sun, Y., Wang, T., Xue, H., Zhang, H., and Zhu, B.: Aerosol and boundary-layer
767 interactions and impact on air quality, *National Science Review*, 4, 810–833, <https://doi.org/10.1093/nsr/nwx117>,
768 2017.
- 769 Liaskos, C. E., Allen, D. J., and Pickering, K. E.: Sensitivity of tropical tropospheric composition to lightning NO_x
770 production as determined by replay simulations with GEOS-5, *Journal of Geophysical Research*, 120, 8512–8534,
771 <https://doi.org/10.1002/2014JD022987>, 2015.
- 772 Liu, Y., Guha, A., Said, R., Williams, E., Lapierre, J., Stock, M., and Heckman, S.: Aerosol Effects on Lightning
773 Characteristics: A Comparison of Polluted and Clean Regimes, *Geophysical Research Letters*, 47, e2019GL086825,
774 <https://doi.org/10.1029/2019GL086825>, 2020.
- 775 Lopez, P.: A lightning parameterization for the ECMWF integrated forecasting system, *Monthly Weather Review*, 144,
776 3057–3075, <https://doi.org/10.1175/MWR-D-16-0026.1>, 2016.
- 777 Manabe, S. and Wetherald, R. T.: The Effects of Doubling the CO₂ Concentration on the climate of a General Circulation
778 Model, *Journal of the Atmospheric Sciences*, 32, 3–15, [https://doi.org/10.1175/1520-](https://doi.org/10.1175/1520-0469(1975)032<0003:TEODTC>2.0.CO;2)
779 0469(1975)032<0003:TEODTC>2.0.CO;2, 1975.
- 780 van Marle, M. J. E., Kloster, S., Magi, B. I., Marlon, J. R., Daniiau, A.-L., Field, R. D., Arneeth, A., Forrest, M., Hantson, S.,
781 Kehrwald, N. M., Knorr, W., Lasslop, G., Li, F., Mangeon, S., Yue, C., Kaiser, J. W., and van der Werf, G. R.:
782 Historic global biomass burning emissions for CMIP6 (BB4CMIP) based on merging satellite observations with



- 783 proxies and fire models (1750–2015), *Geosci. Model Dev.*, 10, 3329–3357, [https://doi.org/10.5194/gmd-10-3329-](https://doi.org/10.5194/gmd-10-3329-2017)
784 2017, 2017.
- 785 McCaul, E. W., Goodman, S. J., LaCasse, K. M., and Cecil, D. J.: Forecasting lightning threat using cloud-resolving model
786 simulations, *Weather and Forecasting*, 24, 709–729, <https://doi.org/10.1175/2008WAF2222152.1>, 2009.
- 787 Meinshausen, M., Vogel, E., Nauels, A., Lorbacher, K., Meinshausen, N., Etheridge, D. M., Fraser, P. J., Montzka, S. A.,
788 Rayner, P. J., Trudinger, C. M., Krummel, P. B., Beyerle, U., Canadell, J. G., Daniel, J. S., Enting, I. G., Law, R. M.,
789 Lunder, C. R., O’Doherty, S., Prinn, R. G., Reimann, S., Rubino, M., Velders, G. J. M., Vollmer, M. K., Wang, R. H.
790 J., and Weiss, R.: Historical greenhouse gas concentrations for climate modelling (CMIP6), *Geoscientific Model*
791 *Development*, 10, 2057–2116, <https://doi.org/10.5194/gmd-10-2057-2017>, 2017.
- 792 Miller, R. L., Schmidt, G. A., Nazarenko, L. S., Tausnev, N., Bauer, S. E., DelGenio, A. D., Kelley, M., Lo, K. K., Ruedy,
793 R., Shindell, D. T., Aleinov, I., Bauer, M., Bleck, R., Canuto, V., Chen, Y., Cheng, Y., Clune, T. L., Faluvegi, G.,
794 Hansen, J. E., Healy, R. J., Kiang, N. Y., Koch, D., Lacis, A. A., LeGrande, A. N., Lerner, J., Menon, S., Oinas, V.,
795 Pérez García-Pando, C., Perlwitz, J. P., Puma, M. J., Rind, D., Romanou, A., Russell, G. L., Sato, M., Sun, S.,
796 Tsigaridis, K., Unger, N., Voulgarakis, A., Yao, M.-S., and Zhang, J.: CMIP5 historical simulations (1850–2012)
797 with GISS ModelE2, *Journal of Advances in Modeling Earth Systems*, 6, 441–478,
798 <https://doi.org/10.1002/2013MS000266>, 2014.
- 799 Murray, L. T.: Lightning NO_x and Impacts on Air Quality, *Current Pollution Reports*, 2, 115–133,
800 <https://doi.org/10.1007/s40726-016-0031-7>, 2016.
- 801 NASA Goddard Institute for Space (NASA/GISS): NASA-GISS GISS-E2-1-G-CC model output prepared for CMIP6 CMIP
802 historical, <https://doi.org/10.22033/ESGF/CMIP6.11762>, 2019.
- 803 Ott, L. E., Pickering, K. E., Stenchikov, G. L., Allen, D. J., DeCaria, A. J., Ridley, B., Lin, R. F., Lang, S., and Tao, W. K.:
804 Production of lightning NO_x and its vertical distribution calculated from three-dimensional cloud-scale chemical
805 transport model simulations, *Journal of Geophysical Research Atmospheres*, 115, 4301,
806 <https://doi.org/10.1029/2009JD011880>, 2010.
- 807 Pinto, O.: Lightning and climate: A review, in: 2013 International Symposium on Lightning Protection (XII SIPDA), 2013
808 International Symposium on Lightning Protection (XII SIPDA), journalAbbreviation: 2013 International Symposium
809 on Lightning Protection (XII SIPDA), 402–404, <https://doi.org/10.1109/SIPDA.2013.6729250>, 2013.
- 810 Price, C. and Rind, D.: A simple lightning parameterization for calculating global lightning distributions, *Journal of*
811 *Geophysical Research*, 97, 9919–9933, <https://doi.org/10.1029/92JD00719>, 1992.
- 812 Price, C. and Rind, D.: What determines the cloud-to-ground lightning fraction in thunderstorms?, *Geophysical Research*
813 *Letters*, 20, 463–466, <https://doi.org/10.1029/93GL00226>, 1993.
- 814 Price, C. and Rind, D.: Possible implications of global climate change on global lightning distributions and frequencies,
815 *Journal of Geophysical Research*, 99, 823–833, <https://doi.org/10.1029/94jd00019>, 1994.
- 816 Rayner, N. A., Parker, D. E., Horton, E. B., Folland, C. K., Alexander, L. V., Rowell, D. P., Kent, E. C., and Kaplan, A.:
817 Global analyses of sea surface temperature, sea ice, and night marine air temperature since the late nineteenth century,
818 *Journal of Geophysical Research: Atmospheres*, 108, <https://doi.org/10.1029/2002jd002670>, 2003.
- 819 Ridley, B. A., Pickering, K. E., and Dye, J. E.: Comments on the parameterization of lightning-produced NO in global
820 chemistry-transport models, *Atmospheric Environment*, 39, 6184–6187,
821 <https://doi.org/10.1016/j.atmosenv.2005.06.054>, 2005.
- 822 Romps, D. M., Seeley, J. T., Vollaro, D., and Molinari, J.: Projected increase in lightning strikes in the united states due to
823 global warming, *Science*, 346, 851–854, <https://doi.org/10.1126/science.1259100>, 2014.
- 824 Sato, M., Hansen, J. E., McCormick, M. P., and Pollack, J. B.: Stratospheric aerosol optical depths, 1850–1990, *Journal of*
825 *Geophysical Research: Atmospheres*, 98, 22987–22994, <https://doi.org/10.1029/93JD02553>, 1993.
- 826 Saunders, C. P. R., Keith, W. D., and Mitzeva, R. P.: The effect of liquid water on thunderstorm charging, *Journal of*
827 *Geophysical Research: Atmospheres*, 96, 11007–11017, <https://doi.org/10.1029/91JD00970>, 1991.
- 828 Schumann, U. and Huntrieser, H.: The global lightning-induced nitrogen oxides source, *Atmospheric Chemistry and Physics*,
829 7, 3823–3907, <https://doi.org/10.5194/acp-7-3823-2007>, 2007.
- 830 Sellar, A. A., Jones, C. G., Mulcahy, J. P., Tang, Y., Yool, A., Wiltshire, A., O’Connor, F. M., Stringer, M., Hill, R.,
831 Palmieri, J., Woodward, S., de Mora, L., Kuhlbrodt, T., Rumbold, S. T., Kelley, D. I., Ellis, R., Johnson, C. E.,
832 Walton, J., Abraham, N. L., Andrews, M. B., Andrews, T., Archibald, A. T., Berthou, S., Burke, E., Blockley, E.,



- 833 Carslaw, K., Dalvi, M., Edwards, J., Folberth, G. A., Gedney, N., Griffiths, P. T., Harper, A. B., Hendry, M. A.,
834 Hewitt, A. J., Johnson, B., Jones, A., Jones, C. D., Keeble, J., Liddicoat, S., Morgenstern, O., Parker, R. J., Predoi, V.,
835 Robertson, E., Siahahaan, A., Smith, R. S., Swaminathan, R., Woodhouse, M. T., Zeng, G., and Zerroukat, M.:
836 UKESM1: Description and Evaluation of the U.K. Earth System Model, *Journal of Advances in Modeling Earth*
837 *Systems*, 11, 4513–4558, <https://doi.org/10.1029/2019MS001739>, 2019.
- 838 Soden, B. J., Wetherald, R. T., Stenchikov, G. L., and Robock, A.: Global Cooling After the Eruption of Mount Pinatubo: A
839 Test of Climate Feedback by Water Vapor, *Science*, 296, 727–730, <https://doi.org/10.1126/science.296.5568.727>,
840 2002.
- 841 Sudo, K. and Akimoto, H.: Global source attribution of tropospheric ozone: Long-range transport from various source
842 regions, *Journal of Geophysical Research Atmospheres*, 112, <https://doi.org/10.1029/2006JD007992>, 2007.
- 843 Sudo, K., Takahashi, M., Kurokawa, J. I., and Akimoto, H.: CHASER: A global chemical model of the troposphere 1. Model
844 description, *Journal of Geophysical Research Atmospheres*, 107, ACH 7-1-ACH 7-20,
845 <https://doi.org/10.1029/2001JD001113>, 2002.
- 846 Takemura, T., Egashira, M., Matsuzawa, K., Ichijo, H., O’Ishi, R., and Abe-Ouchi, A.: A simulation of the global
847 distribution and radiative forcing of soil dust aerosols at the Last Glacial Maximum, *Atmospheric Chemistry and*
848 *Physics*, 9, 3061–3073, <https://doi.org/10.5194/acp-9-3061-2009>, 2009.
- 849 Tan, Y. B., Peng, L., Shi, Z., and Chen, H. R.: Lightning flash density in relation to aerosol over Nanjing (China),
850 *Atmospheric Research*, 174–175, 1–8, <https://doi.org/10.1016/j.atmosres.2016.01.009>, 2016.
- 851 Tang, Y., Rumbold, S., Ellis, R., Kelley, D., Mulcahy, J., Sellar, A., Walton, J., and Jones, C.: MOHC UKESM1.0-LL
852 model output prepared for CMIP6 CMIP historical, <https://doi.org/10.22033/ESGF/CMIP6.6113>, 2019.
- 853 Tost, H.: Chemistry-climate interactions of aerosol nitrate from lightning, *Atmospheric Chemistry and Physics*, 17, 1125–
854 1142, <https://doi.org/10.5194/acp-17-1125-2017>, 2017.
- 855 Veraverbeke, S., Finney, D., Werf, G. van der, Wees, D. van, Xu, W., and Jones, M.: Global attribution of anthropogenic
856 and lightning fires, *Copernicus Meetings*, <https://doi.org/10.5194/egusphere-egu22-1160>, 2022.
- 857 Wang, Q., Li, Z., Guo, J., Zhao, C., and Cribb, M.: The climate impact of aerosols on the lightning flash rate: Is it detectable
858 from long-term measurements?, *Atmospheric Chemistry and Physics*, 18, 12797–12816, <https://doi.org/10.5194/acp-18-12797-2018>, 2018.
- 860 Watanabe, S., Hajima, T., Sudo, K., Nagashima, T., Takemura, T., Okajima, H., Nozawa, T., Kawase, H., Abe, M.,
861 Yokohata, T., Ise, T., Sato, H., Kato, E., Takata, K., Emori, S., and Kawamiya, M.: MIROC-ESM 2010: Model
862 description and basic results of CMIP5-20c3m experiments, *Geoscientific Model Development*, 4, 845–872,
863 <https://doi.org/10.5194/gmd-4-845-2011>, 2011.
- 864 Wild, O.: Liaskos, *Atmospheric Chemistry and Physics*, 7, 2643–2660, <https://doi.org/10.5194/acp-7-2643-2007>, 2007.
- 865 Williams, E. R., Weber, M. E., and Orville, R. E.: The relationship between lightning type and convective state of
866 thunderclouds, *Journal of Geophysical Research: Atmospheres*, 94, 13213–13220,
867 <https://doi.org/10.1029/JD094iD11p13213>, 1989.
- 868 Yang, X., Yao, Z., Li, Z., and Fan, T.: Heavy air pollution suppresses summer thunderstorms in central China, *Journal of*
869 *Atmospheric and Solar-Terrestrial Physics*, 95–96, 28–40, <https://doi.org/10.1016/j.jastp.2012.12.023>, 2013.
- 870 Yuan, T., Remer, L. A., Pickering, K. E., and Yu, H.: Observational evidence of aerosol enhancement of lightning activity
871 and convective invigoration, *Geophysical Research Letters*, 38, 4701, <https://doi.org/10.1029/2010GL046052>, 2011.
- 872 Zeng, G., Pyle, J. A., and Young, P. J.: Impact of climate change on tropospheric ozone and its global budgets, *Atmospheric*
873 *Chemistry and Physics*, 8, 369–387, <https://doi.org/10.5194/acp-8-369-2008>, 2008.

875